

Prepared in cooperation with the Bureau of Land Management

Geology, Geochemistry, and Geophysics of the Fry Canyon Uranium/Copper Project Site, Southeastern Utah— Indications of Contaminant Migration



Scientific Investigations Report 2010–5075

Geology, Geochemistry, and Geophysics of the Fry Canyon Uranium/Copper Project Site, Southeastern Utah—Indications of Contaminant Migration

By James K. Otton, Robert A. Zielinski, and Robert J. Horton

Prepared in cooperation with the Bureau of Land Management

Scientific Investigations Report 2010–5075

U.S. Department of the Interior
U.S. Geological Survey

U.S. Department of the Interior
KEN SALAZAR, Secretary

U.S. Geological Survey
Marcia K. McNutt, Director

U.S. Geological Survey, Reston, Virginia: 2010

For more information on the USGS—the Federal source for science about the Earth, its natural and living resources, natural hazards, and the environment, visit <http://www.usgs.gov> or call 1-888-ASK-USGS

For an overview of USGS information products, including maps, imagery, and publications, visit <http://www.usgs.gov/pubprod>

To order this and other USGS information products, visit <http://store.usgs.gov>

Any use of trade, product, or firm names is for descriptive purposes only and does not imply endorsement by the U.S. Government.

Although this report is in the public domain, permission must be secured from the individual copyright owners to reproduce any copyrighted materials contained within this report.

Suggested citation:

Otton, J.K., Zielinski, R.A., and Horton, R.J., 2010, Geology, geochemistry, and geophysics of the Fry Canyon uranium/copper project site, southeastern Utah—Indications of contaminant migration: U.S. Geological Survey Scientific Investigations Report 2010–5075, 39 p.

Contents

Abstract.....	1
Introduction.....	1
Methods.....	3
Mapping.....	3
Sampling.....	3
Analyses.....	3
Waters.....	3
Sediments.....	5
Electromagnetic Survey.....	5
Direct-Current Electrical Resistivity Survey.....	5
Survey Instrumentation.....	6
Resistivity Data Processing.....	7
Geology, Geophysics, and Geochemistry.....	7
Stratigraphy.....	7
Cross Sections—Geologic Relations and Interpretations.....	11
Direct-Current Resistivity Survey.....	13
Interpretation.....	14
Line FC-1.....	14
Line FC-3.....	17
Line FC-2.....	17
Line FC-4.....	18
Structure.....	18
General Chemical Character of Water.....	19
Aqueous Geochemistry of Uranium.....	22
Spatial Distribution of Dissolved Uranium.....	23
Uranium Isotopes.....	23
Sulfur Isotopes.....	25
Sediment Chemistry and Mineralogy.....	26
Summary and Conclusions.....	29
Acknowledgments.....	31
References Cited.....	31
Appendix 1. Description of disturbed areas.....	35
Appendix 2. Apparent resistivity pseudosections and inversion results.....	37

Figures

1. Maps showing locations of the Fry Canyon project site in San Juan County, southeastern Utah, and areas of geologic mapping.....	2
2. Map of a portion of Fry Canyon, southeastern Utah, showing the location of the Fry Canyon project site and locations where surface water and groundwater and stream sediments were collected.....	5
3. Location of dc resistivity lines FC1-4 at the Fry Canyon project site.....	6
4. Geologic map of the ranch area north of the Fry Canyon project site.....	8
5. Geologic map of the Fry Canyon project site and vicinity.....	9

6.	Geologic map of the Fry Spring area south of the Fry Canyon project site.....	10
7.	Cross section <i>A–A'</i> across the modern stream channel of Fry Creek and the bench to the south, at the position of the berm between ponds 4 and 5.....	12
8.	Cross section <i>B–B'</i> across the valley floor of Fry Creek north of the Fry Canyon project site at the location of a washed-out road.....	12
9.	Cross section <i>C–C'</i> across the valley floor of Fry Creek at the location of the cottonwood tree well field.....	13
10.	Direct-current resistivity profile for Fry Canyon line FC–1.....	14
11.	Direct-current resistivity profile for Fry Canyon line FC–3.....	15
12.	Direct-current resistivity profile for Fry Canyon line FC–2.....	15
13.	Direct-current resistivity profile for Fry Canyon line FC–4.....	16
14.	Pie diagrams showing the relative percentages of major cations and anions (on a milliequivalent basis) in well W15 from the center of the contaminant plume and well W16, which is more representative of other contaminated water samples collected in this study.....	21
15.	Plot showing the relative abundance of major dissolved U(VI) species as a function of pH in waters of this study.....	22
16.	Plot showing degree of saturation of sampled waters with respect to a variety of minerals, including uranium minerals.....	23
17.	Plot of dissolved uranium concentration as a function of sampling-site location along the main stem of Fry Creek.....	23
18.	Photograph of view upstream from water-sampling site W1 in Fry Creek.....	24
19.	Plot of $^{234}\text{U}/^{238}\text{U}$ activity ratio (AR) of water as a function of sampling-site location along the main stem of Fry Creek.....	24
20.	Plot of $^{234}\text{U}/^{238}\text{U}$ activity ratio (AR) compared to dissolved uranium concentration in waters of this study.....	25
21.	Plot of $\delta^{34}\text{S}$ of dissolved sulfate compared to dissolved sulfate concentration in waters of this study.....	25
22.	Photographs of variably altered pyrite and chalcopyrite grains in the magnetic fraction of the 60–120 mesh size fraction of tailings sample T1 (<i>A–F</i>), and in downstream sediment S5 (<i>G–K</i>), and S6 (<i>L</i>).....	27
23.	Backscatter electron image (BSE) and corresponding X-ray intensity maps for copper, sulfur, and iron for a portion (8 square millimeters) of thin section T1 containing magnetic minerals from the tailings location.....	29
24.	Map of the Fry Canyon project study area showing modern channel and possible position of the paleochannel along the floor of Fry Creek.....	30

Appendix Figures

25. Supporting information for direct-current resistivity profile FC-1	37
26. Supporting information for direct-current resistivity profile FC-3	38
27. Supporting information for direct-current resistivity profile FC-2	38
28. Supporting information for direct-current resistivity profile FC-4	39

Tables

1. UTM coordinates of Fry Canyon direct-current resistivity profiles.....	7
2. Chemical and isotopic composition of surface water, seeps, springs, and wells, Fry Canyon, Utah.....	19
3. Concentrations of selected trace elements ($\mu\text{g/g}$) in the 60–120 mesh size fraction of tailings and stream sediments, Fry Canyon, Utah.....	26

Geology, Geochemistry, and Geophysics of the Fry Canyon Uranium/Copper Project Site, Southeastern Utah—Indications of Contaminant Migration

By James K. Otton, Robert A. Zielinski, and Robert J. Horton

Abstract

The Fry Canyon uranium/copper project site in San Juan County, southeastern Utah, was affected by the historical (1957–68) processing of uranium and copper-uranium ores. Relict uranium tailings and related ponds, and a large copper heap-leach pile at the site represent point sources of uranium and copper to local soils, surface water, and groundwater. This study was designed to establish the nature, extent, and pathways of contaminant dispersion. The methods used in this study are applicable at other sites of uranium mining, milling, or processing.

The uranium tailings and associated ponds sit on a bench that is as much as 4.25 meters above the level of the adjacent modern channel of Fry Creek. The copper heap leach pile sits on bedrock just south of this bench. Contaminated groundwater from the ponds and other nearby sites moves downvalley and enters the modern alluvium of adjacent Fry Creek, its surface water, and also a broader, deeper paleochannel that underlies the modern creek channel and adjacent benches and stream terraces. The northern extent of contaminated groundwater is uncertain from geochemical data beyond an area of monitoring wells about 300 meters north of the site. Contaminated surface water extends to the State highway bridge. Some uranium-contaminated groundwater may also enter underlying bedrock of the Permian Cedar Mesa Sandstone along fracture zones.

Four dc-resistivity surveys perpendicular to the valley trend were run across the channel and its adjacent stream terraces north of the heap-leach pile and ponds. Two surveys were done in a small field of monitoring wells and two in areas untested by borings to the north of the well field. Bedrock intercepts, salt distribution, and lithologic information from the wells and surface observations in the well field aided interpretation of the geophysical profiles there and allowed interpretation of the two profiles not tested by wells. The geophysical data for the two profiles to the north of the well field suggest that the paleochannel persists at least 900 m to the north of the heap leach and pond sites. Contamination of groundwater beneath the stream terraces may extend at least that far.

Fry Creek surface water (six samples), seeps and springs (six samples), and wells (eight samples) were collected during a dry period of April 16–19, 2007. The most uranium-rich (18.7 milligrams per liter) well water on the site displays distinctive Ca-Mg-SO₄-dominant chemistry indicating the legacy of heap leaching copper-uranium ores with sulfuric acid. This same water has strongly negative $\delta^{34}\text{S}$ of sulfate (–13.3 per mil) compared to most local waters of –2.4 to –5.4 per mil. Dissolved uranium species in all sampled waters are dominantly U(VI)-carbonate complexes. All waters are undersaturated with respect to U(VI) minerals. The average ²³⁴U/²³⁸U activity ratio (AR) in four well waters from the site (0.939±0.011) is different from that of seven upstream waters (1.235±0.069). This isotopic contrast permits quantitative estimates of mixing of site-derived uranium with natural uranium in waters collected downstream. At the time of sampling, uranium in downstream surface water was mostly (about 67 percent) site-derived and subject to further concentration by evaporation. Three monitoring wells located approximately 0.4 kilometer downstream contained dominantly (78–87 percent) site-derived uranium. Distinctive particles of chalcopyrite (CuFeS) and variably weathered pyrite (FeS₂) are present in tailings at the stream edge on the site and are identified in stream sediments 1.3 kilometers downstream, based on inspection of polished grain mounts of magnetic mineral separates.

Introduction

Uranium ore upgrading (1957–1960) and sulfuric acid heap leaching of copper-uranium ores (1963–1968) have contaminated water and land at the Fry Canyon uranium/copper project site in San Juan County, southeastern Utah (fig. 1). The site is managed by the Bureau of Land Management (BLM), which is conducting site investigations to support final plans for site remediation. A plume of contaminated groundwater beneath the site contains elevated concentrations of dissolved uranium (1,000–20,000 micrograms per liter [µg/L]), copper (<4–20 µg/L), and sulfate (1,200–1,900 milligrams per liter

2 Geology, Geochemistry, and Geophysics of the Fry Canyon Uranium/Copper Project Site, Southeastern Utah

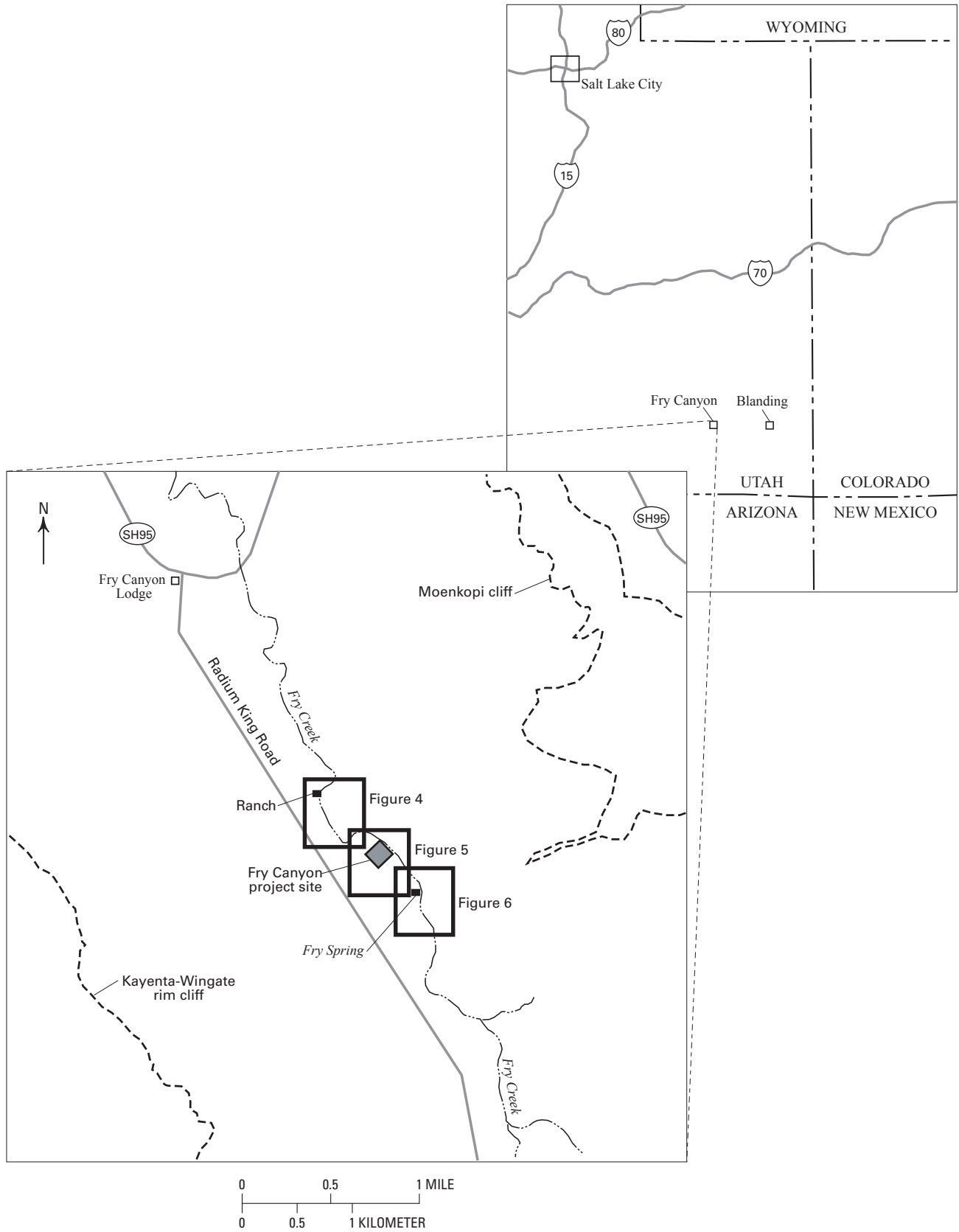


Figure 1. Maps showing locations of the Fry Canyon project site in San Juan County, southeastern Utah, and areas of geologic mapping (figs. 4–6).

[mg/L]), and well waters 0.5 km downgradient from the site contain greater than 100 $\mu\text{g/L}$ uranium (Wilkowski and others, 2002). Features on the site include an abandoned copper heap-leach pile and ponds and associated uranium tailings that contain uranium, copper, and other elements subject to mobilization by wind and water. Field studies by the U.S. Geological Survey (USGS) during 1996–2006 investigated the effectiveness of several prototype permeable reactive barriers (PRB) to treat the contaminant plume (Naftz and others, 1999, 2000, 2002, 2006).

The purpose of this report is to present additional geologic, chemical, geophysical, mineralogic, and isotopic data that indicate some of the mechanisms and pathways for offsite dispersion of contaminants and the effects on the surrounding environment. The new data include (1) geologic maps and cross sections that show areas upstream and downstream from the site and identify geologic controls on offsite movement of groundwater, (2) geophysical data that define older channel gravels that serve as reservoirs for contaminated groundwater and pathways for its movement downvalley, (3) chemical data that indicate the aqueous geochemistry of uranium in local waters and possible chemical controls on uranium mobility, (4) isotopic data for dissolved uranium that permit more accurate and sensitive tracing of site-derived uranium in local waters, and (5) chemical and mineralogical observations of stream sediments that permit tracing of site-derived sulfide minerals in the streambed of Fry Creek.

Methods

Mapping

Three partly overlapping aerial photographs derived from Google Earth were used as base maps for geologic mapping. Locations of the three mapped areas, each of which covered a tract approximately 520 m east-west by 450 m north-south, are shown in figure 1. They are (1) the area around a ranch north of the project site, (2) the project site (shaded area, fig. 1, also referred to as the ore-processing site), and (3) the area around Fry Spring south of the project site. The photographs have not been georeferenced, so there is some scale distortion near the margins of each image. Three cross sections were drawn across Fry Creek at selected locations near the project site by using a tape measure and hand level to supplement the geologic maps in showing the detailed geologic relations at and near the project site. Lithologic data from monitoring wells were used in two of the cross sections.

Sampling

Twenty water samples and 9 sediment samples (fig. 2) were collected in the drainage of Fry Creek during a dry period spanning April 16–19, 2007. This sampling provided a snapshot of conditions presumed to be typical for this small first-order stream located in a semiarid environment. In the absence of recent rainfall, normal streamflow of less than

2.8 liters per second (L/s) is largely sustained by returns of groundwater as seeps and springs (Wilkowski and others, 2002). Sampling within and adjacent to Fry Creek included locations upstream from the Fry Canyon project site and successive downstream locations over a total stream reach of approximately 4 km (fig. 2). Water samples included the main channel of Fry Creek (six samples), springs and seeps (six samples), and shallow (less than 7 m) plume wells and monitoring wells (eight samples). Wells included one upstream “background” well near Fry Spring (W19), four plume wells within the pond and tailings area on the bench (W15–W18), and three monitoring wells on a stream terrace downvalley from the project site (W13, W14, W20). The streamflow was continuous from the uppermost sampling site (W1) to a sampling site approximately 1.3 km downstream from the project site (W10). Two other stream samples (W11, W12) were collected farther downstream where surface flow reemerged from beneath a dry streambed.

Water temperature, pH, and specific conductance were measured at the time of sampling. An additional 250 milliliters (mL) of each water sample was collected in a field-rinsed polyethylene bottle and placed under refrigeration for transport to the laboratory. Wells were sampled using a peristaltic pump, and water was collected only after stabilization of temperature and specific conductance. This required pumping of approximately 10 L of water before sampling.

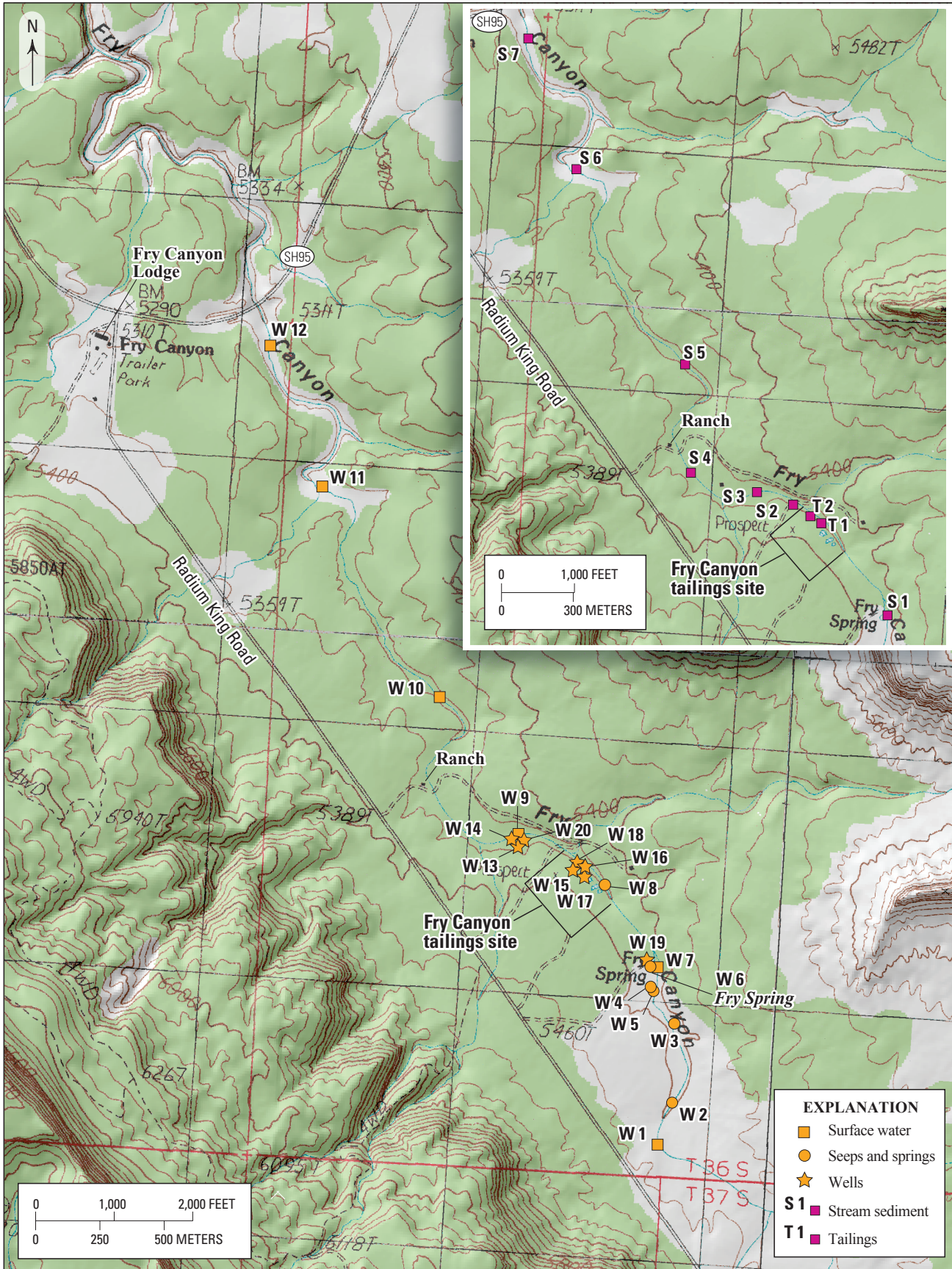
Stream sediments (seven samples) were collected at locations that generally corresponded to locations of surface-water samples (fig. 2, inset). At each location, 2–3 kilograms (kg) of dominantly sand- to silt-sized moist sediment were collected by combining samples from several locations within the active stream channel. Two grab samples of sand- to silt-sized tailings were collected from a steep slope of tailings adjacent to Fry Creek (T1, T2, fig. 2, inset). The nose of this tailings slope is submerged and potentially mobilized by stream waters during intermittent flash floods that can increase stream discharge to over 8.5 cubic meters per second (m^3/s) (Wilkowski and others, 2002). Sediments were collected with plastic scoops and stored in sealed polyethylene bags.

Analyses

Waters

Water samples were delivered to USGS laboratories in Denver and filtered through cellulose acetate filter membranes with 0.45-micrometer (μm) openings, under pressure from nitrogen gas. Approximately 60 mL of each sample was acidified to $\text{pH} < 2$ with high-purity nitric acid and submitted for analyses of major dissolved cations by inductively coupled plasma–atomic emission spectrometry (ICP–AES), and for analyses of selected minor and trace elements by inductively coupled plasma–mass spectrometry (ICP–MS) (Briggs, 2002; Lamothe and others, 2002). Remaining amounts of acidified waters were used for determinations of uranium isotopic composition. Filtered but unacidified portions of each water

4 Geology, Geochemistry, and Geophysics of the Fry Canyon Uranium/Copper Project Site, Southeastern Utah



sample were used for determination of carbonate alkalinity by titration with standard acid, for determination of other major dissolved anions by ion chromatography (IC), and for measurements of sulfur isotope composition. Estimated accuracy and precision of the chemical analyses, expressed as relative standard deviation (RSD), were generally better than 5 percent for alkalinity and major cations and anions and 10 percent for minor and trace elements.

The concentration and isotopic composition of dissolved uranium was determined by passing a 10-mL aliquot of acidified water through a column of uranium-specific resin (UTEVA[®]) and analyzing the eluted uranium by sector field ICP-MS. The isotopic ratio of interest in this study is the ²³⁴U/²³⁸U activity ratio (AR). This ratio of (radio)activity concentrations is calculated from the measured mass ratio of the two isotopes. Mass ratios are first corrected for instrument blanks and instrument-based mass discrimination. Estimated accuracy and precision of the technique based on replicate measurements of standards is ±5 percent (RSD) for uranium concentration and better than ±1 percent for AR values.

The concentration and isotopic composition of dissolved sulfur (as sulfate) was determined by (1) concentrating dissolved sulfate in a precipitate of barium sulfate and (2) combusting the barium sulfate in an elemental analyzer and directing the produced SO₂ gas into an in-line continuous-flow mass spectrometer. The sulfur isotopic composition is reported as a δ³⁴S value, calculated as follows:

$$\delta^{34}\text{S} \text{ (in per mil, ‰)} = (R_{\text{sample}}/R_{\text{standard}} - 1) \times 1,000$$

where

R is the atomic ³⁴S/³²S ratio and the standard is Vienna Canyon Diablo troilite (V-CDT).

Accuracy and precision of the measurements was ±0.2 per mil based on multiple determinations of sulfur isotopic standards (NBS-127, IAEA-S-5, and IAEA-S-6).

Sediments

Sediments were air-dried at 40°C and then passed through a stainless steel sieve with 2-millimeter (mm) openings, with material coarser than 2 mm discarded. Approximately 500 g of each sediment was passed through a series of stainless steel sieves to produce the following size fractions: 2.0–0.25 mm (10–60 mesh), 0.25–0.125 mm (60–120 mesh), and <0.125 mm (<120 mesh). The 60–120 mesh size fraction of each sample was observed under a binocular microscope to initially characterize constituent minerals. Approximately

10 g of the 60–120 mesh fraction was ground to a fine powder in a ceramic ball mill, and 0.1-g aliquots were dissolved in a mixture of mineral acids. The acid digests were analyzed for copper, uranium, and other trace elements by ICP-MS.

Approximately 35 g of each 60–120 mesh fraction was screened with a hand magnet to remove (rare) magnetite and then passed through a Franz isodynamic magnetic separator (1.7 amperes, 15-degree tilt angle) to concentrate other magnetic minerals, including copper sulfide minerals (Rosenblum and Brownfield, 1999). Numerous grains of each magnetic concentrate were mounted as a closely packed assemblage on a 16- by 16-mm area of a polished thin section. The entire area of each thin section was viewed in 1- by 1-mm area increments at 160 times magnification under reflected light illumination, using oil-immersion objectives. The total number of highly reflective and variably altered sulfide grains on each thin section was recorded.

The thin section of tailings sample T1 was also scanned for grains containing high concentrations of copper using a JEOL JXA 8900 electron microprobe operating at 15-kilovolt accelerating voltage, 50-nanoampere current. Beam diameter was 10 μm. Backscatter electron image (BEI) mode was used to identify (brightest) grains containing high concentrations of heavy elements. Wavelength dispersive X-ray intensity maps of copper, iron, and sulfur were also acquired to distinguish copper-rich minerals from pyrite and iron oxides. Each map area covered approximately 8 mm² and consisted of 800 × 800 pixels.

Electromagnetic Survey

Direct-Current Electrical Resistivity Survey

Direct-current (dc) resistivity surveys were conducted across the Fry Canyon stream channel. The purpose of the Fry Canyon resistivity surveys was to help delineate the stream's bedrock channel downgradient from the mill site. Parts of the bedrock channel may coincide with the modern stream channel, but parts may be buried underneath adjacent benches and stream terraces. The sediment cover on the benches and stream terraces obscures the location of the bedrock channel, which may be a significant groundwater conduit for contaminant migration below the site. The basic premise for using the dc-resistivity method is that a resistivity contrast should exist between the surficial unconsolidated sediment and the underlying bedrock.

Resistivity is the property of a material to resist the flow of electric current. Resistivity is the inverse of electrical conductivity. Resistivity units are ohm-meters (ohm-m). The resistivity of rock and sediment is dependent on several factors including the amount of water present, porosity, the amount of total dissolved solids (TDS) in pore water, and mineral composition of the sediment or bedrock. The amount and TDS of pore water are typically the dominant factors that determine geologic media's resistivity. All other factors being equal, dry

Figure 2 (facing page). Map of a portion of Fry Canyon, southeastern Utah, showing the location of the Fry Canyon project site and locations where surface water and groundwater and stream sediments (S1–7, inset) were collected.

6 Geology, Geochemistry, and Geophysics of the Fry Canyon Uranium/Copper Project Site, Southeastern Utah

rock is more resistive than saturated rock, and rock saturated with low-TDS water is more resistive than rock saturated with high-TDS water. The presence of electrically conductive minerals, such as clays (that is, montmorillonite) and salts, typically results in a lower measured resistivity.

To determine if detectable resistivity contrasts were present at the site, three vertical electrical soundings (VES) were first conducted (Robert Horton, unpub. data, 2007). The VES data indicated conductive over resistive sections, interpreted as wet, often saline, sediment over variably saturated bedrock. Moderate resistivity contrasts observed in the VES data suggested that dc-resistivity profiling could delineate the sediment/bedrock contact.

Based on the encouraging results of the VES measurements, four detailed dc-resistivity profiles were planned and conducted across the stream valley in areas suspected of

having a buried bedrock channel based on the geomorphology and drillhole intercepts of bedrock on terraces that were below bedrock in the modern stream channel. Figure 3 shows the locations of the resistivity profiles.

Survey Instrumentation

For this project, two-dimensional (2-D) dc-resistivity-profile data were collected using a multielectrode Advanced Geosciences, Inc., SuperSting R8 resistivity/IP system. The standard survey setup was to lay out up to 100 stainless steel electrodes 1 m apart along a relatively straight line. The electrodes, which are similar to tent stakes, are pounded into the ground then connected to cables attached to the R8 transmitter/receiver unit. The electrodes were watered with saltwater to



Figure 3. Location of dc resistivity lines FC1–4 at the Fry Canyon project site (shown as gray square in fig. 1).

increase their electrical contact with the ground. The R8 unit was programmed to transmit a 1,000-mA (milliampere) pulse. For each measurement, two readings were made, with the average value being used to calculate the apparent resistivity.

The resistivity data presented here were collected using the inverse Schlumberger array. This array type was chosen because it has good signal-to-noise characteristics relative to other array types (that is, dipole-dipole). To measure the entire profile, the R8 unit sequentially switches the transmitter and receiver electrodes along the survey line by following instructions in a command file. When the R8 finishes collecting data from the existing electrodes, the profile can be extended by moving “used” electrodes from the start of the line to new positions beyond the end of the line. This technique, known as “roll along,” allows for the collection of data along a long, continuous profile. Line 2 used this roll-along technique to extend the line to 128 m.

To determine the position and elevation of the electrodes, the resistivity lines were surveyed using a Trimble R8 global positioning system (GPS). For this survey, the average relative horizontal precision of the GPS locations is 0.008 m (range 0.004–0.031 m), whereas the average relative vertical precision is 0.014 m (range 0.008–0.069 m). Table 1 gives the starting and ending GPS position of each line in UTM, zone 12 coordinates.

Resistivity Data Processing

The resistivity data were processed using the computer program EarthImager 2D (Advanced Geosciences, Inc., 2003). The program is a 2-D inversion routine that takes the observed apparent resistivity data and produces 2-D cross sections that show “true” resistivity as a function of depth. These 2-D, topography-corrected resistivity cross sections are the basis for the subsurface interpretations.

For each inversion, two data files are used including the observed apparent-resistivity data file and a terrain file containing position and elevation data. Using the 2-D geometry of the survey line, the inversion minimizes the root mean square (RMS) error between the observed apparent resistivity and the resistivity calculated from the inverted model. To minimize the

Table 1. UTM coordinates of Fry Canyon direct-current resistivity profiles.

[m, meters]

Line/Position	UTM Northing	UTM Easting	Elevation (meters)
FC-1 0m	4163734.689	576129.146	1,615.655
FC-1 100m	4163832.334	576131.525	1,611.198
FC-2 0m	4163833.353	575876.864	1,609.516
FC-2 128m	4163918.701	575946.202	1,614.469
FC-3 0m	4163750.790	576126.920	1,618.020
FC-3 64m	4163810.939	576122.667	1,613.233
FC-4 0m	4164221.329	575789.047	1,612.621
FC-4 100m	4164272.514	575871.901	1,603.650

RMS error, sequential inversions were run. After each inversion, poorly fit data points are identified and removed on the basis of the percentage misfit value between the measured and calculated apparent resistivity. Typically, the data were sequentially inverted until the RMS error was less than 10 percent.

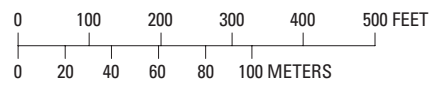
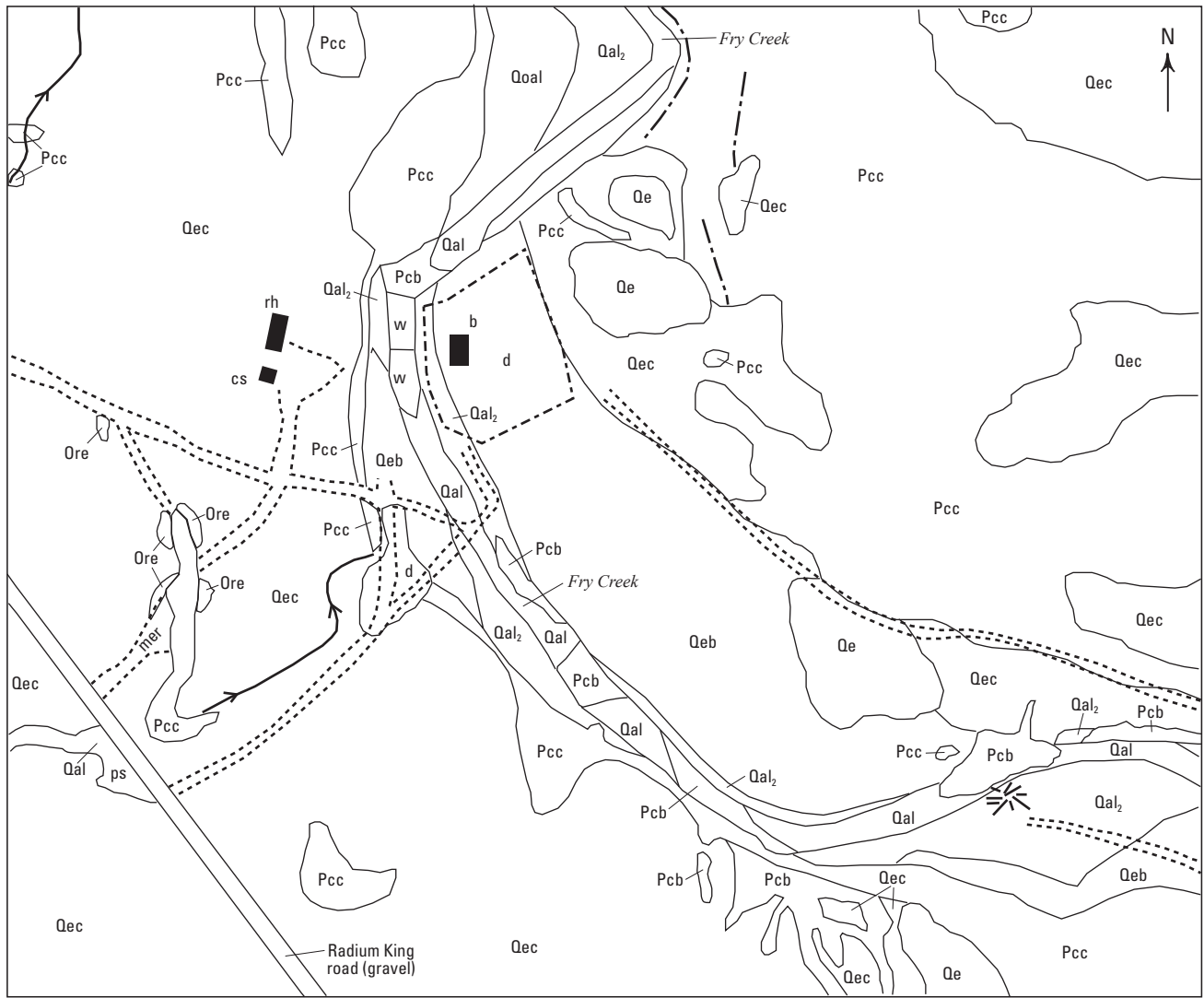
It is important to note that the resistivity data were collected in three-dimensional (3-D) space. If subsurface 3-D heterogeneities are present, the 2-D interpretation may contain errors in the location and size of anomalies. The magnitude of these errors depends on the distance the 3-D heterogeneities are offset from the survey line. The 3-D errors decrease as the distance from the line increases.

Geology, Geophysics, and Geochemistry

Stratigraphy

The geology of the site is characterized by bedrock composed of well-consolidated sandstone, siltstone, and mudstone of the Cedar Mesa Sandstone Member of the Cutler Formation (hereinafter referred to as the “Cedar Mesa sandstone”) of Permian age (Pcc and Pcb in figs. 4–6; Thaden and others, 1964). Sandstone dominates and forms thick, stacked beds composed of crossbedded sandstone that were deposited during the Permian in a large dune field. Interbedded with these sandstones are thinner siltstones and mudstones formed by sediment deposited in interdune low areas. The thin siltstone and mudstone beds tend to weather readily; thus, the thicker sandstone beds form stairstepped ledges that extend away from Fry Creek up the valley slope to the contact with the overlying Organ Rock Member of the Cutler Formation (see bedrock ledges exposed in the minimally disturbed outcrop area southeast of the ore-processing site, dash-dot lines in the map unit Pcc southeast of the area labeled “d” in fig. 5). Along the stream channel and in a few upland areas, the sandstone forms “balds” almost completely devoid of vegetation, eolian sand, colluvium, or alluvium (Pcb in figs. 4–6). The map unit descriptor Pcc is used wherever the covering of surficial sediments is thin and sandstone is exposed almost continuously.

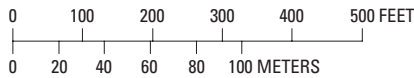
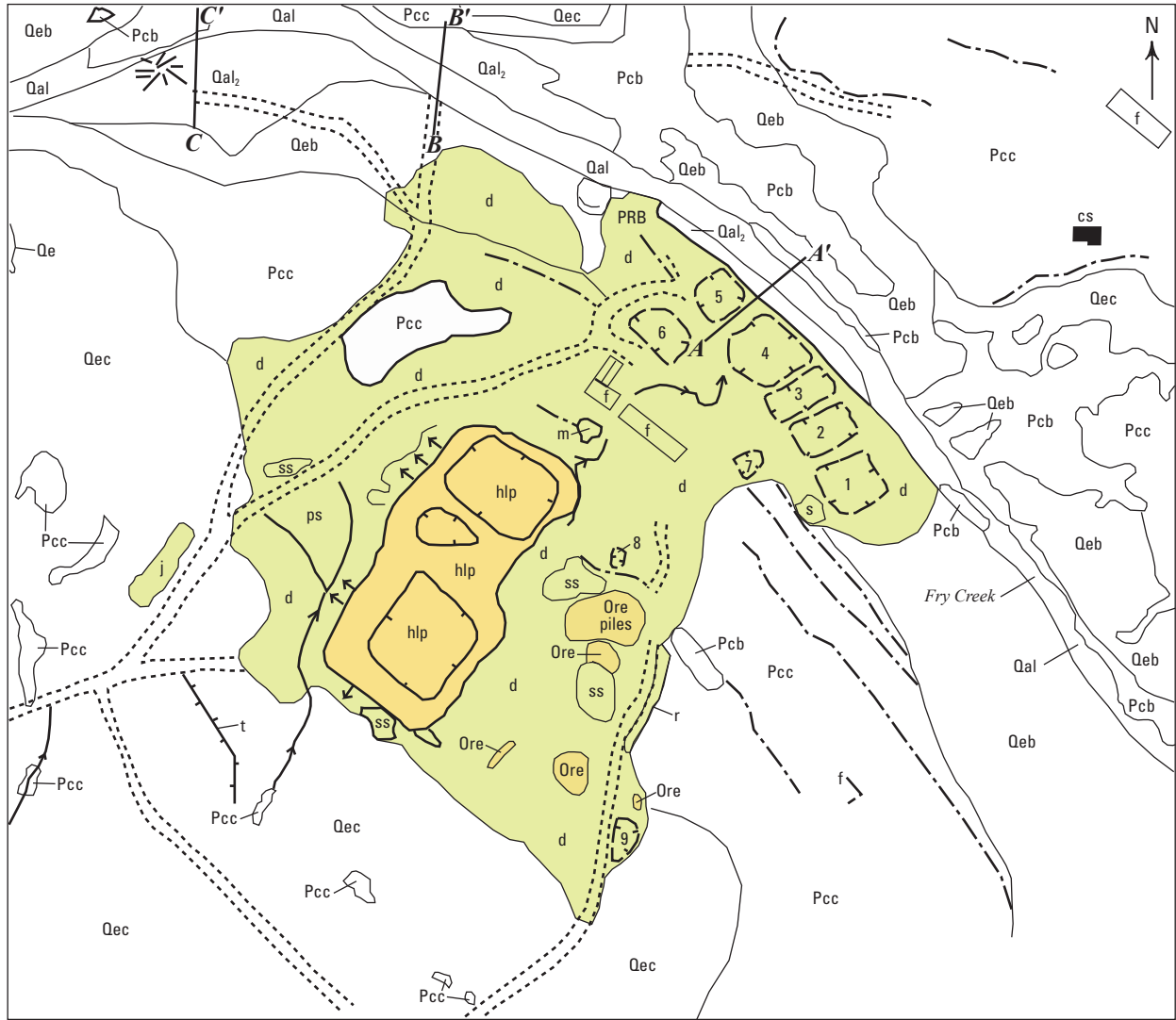
Along the active stream channel, cutbank cliffs have formed locally to expose basal stratified gravels that vary from well-sorted granule and pebble gravel to poorly sorted boulder gravel containing sandstone boulders as much as 1.5–3.0 m across; exposures are too limited, however, for the gravels to be mapped as a separate unit. These gravels contain mixed subangular to well-rounded clasts, eroded from sedimentary rocks in the Fry Creek drainage basin. Because of their proximity to the flowing stream channel, the clasts are commonly coated with soluble salts (probably sulfate salts) and also exhibit imbrications, which indicates a flow direction similar to the modern stream channel.



EXPLANATION

Qal	Recent alluvium	d	Disturbed areas		Gully trace
Qal ₂	Recent alluvial terraces 2–5 ft above modern channel	ps	Ponded sediment		Large cottonwood tree
Qoal	Quaternary to Recent older alluvium with dissected eolian sand surface layer	w	Ponded water (4/2007)		Road
Qe	Quaternary to Holocene eolian sand	rh	Ranch house		Sandstone ledges
Qec, Qeb	Quaternary to Holocene eolian sand and colluvium; Qeb, areas where unit forms a bench along Fry Creek	cs	Car shed		Fence
Pcc, Pcb	Cedar Mesa Sandstone Member of the Permian Cutler Fm.; Pcb, distinctive bald outcrop areas	b	Barn		
		mer	Main entry road to ranch		

Figure 4. Geologic map of the ranch area north of the Fry Canyon project site. Solid rectangles indicate ranch buildings.



EXPLANATION

<table border="1"> <tr><td>Qal</td><td>Recent alluvium</td></tr> <tr><td>Qal₂</td><td>Recent alluvial terraces 2–5 ft above modern channel</td></tr> <tr><td>Qe</td><td>Quaternary to Holocene eolian sand</td></tr> <tr><td>Qec, Qeb</td><td>Quaternary to Holocene eolian sand and colluvium; Qeb, areas where unit forms a bench along Fry Creek</td></tr> <tr><td>Pcc, Pcb</td><td>Cedar Mesa Sandstone Member of the Permian Cutler Fm.; Pcb, distinctive bald outcrop areas</td></tr> </table>	Qal	Recent alluvium	Qal ₂	Recent alluvial terraces 2–5 ft above modern channel	Qe	Quaternary to Holocene eolian sand	Qec, Qeb	Quaternary to Holocene eolian sand and colluvium; Qeb, areas where unit forms a bench along Fry Creek	Pcc, Pcb	Cedar Mesa Sandstone Member of the Permian Cutler Fm.; Pcb, distinctive bald outcrop areas	<table border="0"> <tr><td>d</td><td>Disturbed areas</td></tr> <tr><td>f</td><td>Foundations</td></tr> <tr><td>ps</td><td>Ponded sediment</td></tr> <tr><td>cs</td><td>“Cowboy” shack</td></tr> <tr><td>ss</td><td>Sandstone exposures in disturbed areas</td></tr> <tr><td>t</td><td>Trench</td></tr> <tr><td>r</td><td>Sandstone rubble</td></tr> <tr><td>hlp</td><td>Heap-leach pile</td></tr> <tr><td>j</td><td>Junk pile</td></tr> <tr><td>m</td><td>Rusted metal scrap</td></tr> <tr><td>s</td><td>Slime pile</td></tr> </table>	d	Disturbed areas	f	Foundations	ps	Ponded sediment	cs	“Cowboy” shack	ss	Sandstone exposures in disturbed areas	t	Trench	r	Sandstone rubble	hlp	Heap-leach pile	j	Junk pile	m	Rusted metal scrap	s	Slime pile	<table border="0"> <tr><td></td><td>Gully trace</td></tr> <tr><td></td><td>Outwash from pile</td></tr> <tr><td></td><td>Pits in disturbed area (numbered)</td></tr> <tr><td></td><td>Large cottonwood tree</td></tr> <tr><td></td><td>Road</td></tr> <tr><td></td><td>Sandstone ledges</td></tr> <tr><td></td><td>Cross-section location</td></tr> </table>		Gully trace		Outwash from pile		Pits in disturbed area (numbered)		Large cottonwood tree		Road		Sandstone ledges		Cross-section location
Qal	Recent alluvium																																															
Qal ₂	Recent alluvial terraces 2–5 ft above modern channel																																															
Qe	Quaternary to Holocene eolian sand																																															
Qec, Qeb	Quaternary to Holocene eolian sand and colluvium; Qeb, areas where unit forms a bench along Fry Creek																																															
Pcc, Pcb	Cedar Mesa Sandstone Member of the Permian Cutler Fm.; Pcb, distinctive bald outcrop areas																																															
d	Disturbed areas																																															
f	Foundations																																															
ps	Ponded sediment																																															
cs	“Cowboy” shack																																															
ss	Sandstone exposures in disturbed areas																																															
t	Trench																																															
r	Sandstone rubble																																															
hlp	Heap-leach pile																																															
j	Junk pile																																															
m	Rusted metal scrap																																															
s	Slime pile																																															
	Gully trace																																															
	Outwash from pile																																															
	Pits in disturbed area (numbered)																																															
	Large cottonwood tree																																															
	Road																																															
	Sandstone ledges																																															
	Cross-section location																																															

Figure 5. Geologic map of the Fry Canyon project site (colored area) and vicinity. The locations of cross sections A–A', B–B', and C–C' are shown. PRB, location of the permeable reactive barrier. Numbers indicate uranium waste ponds.

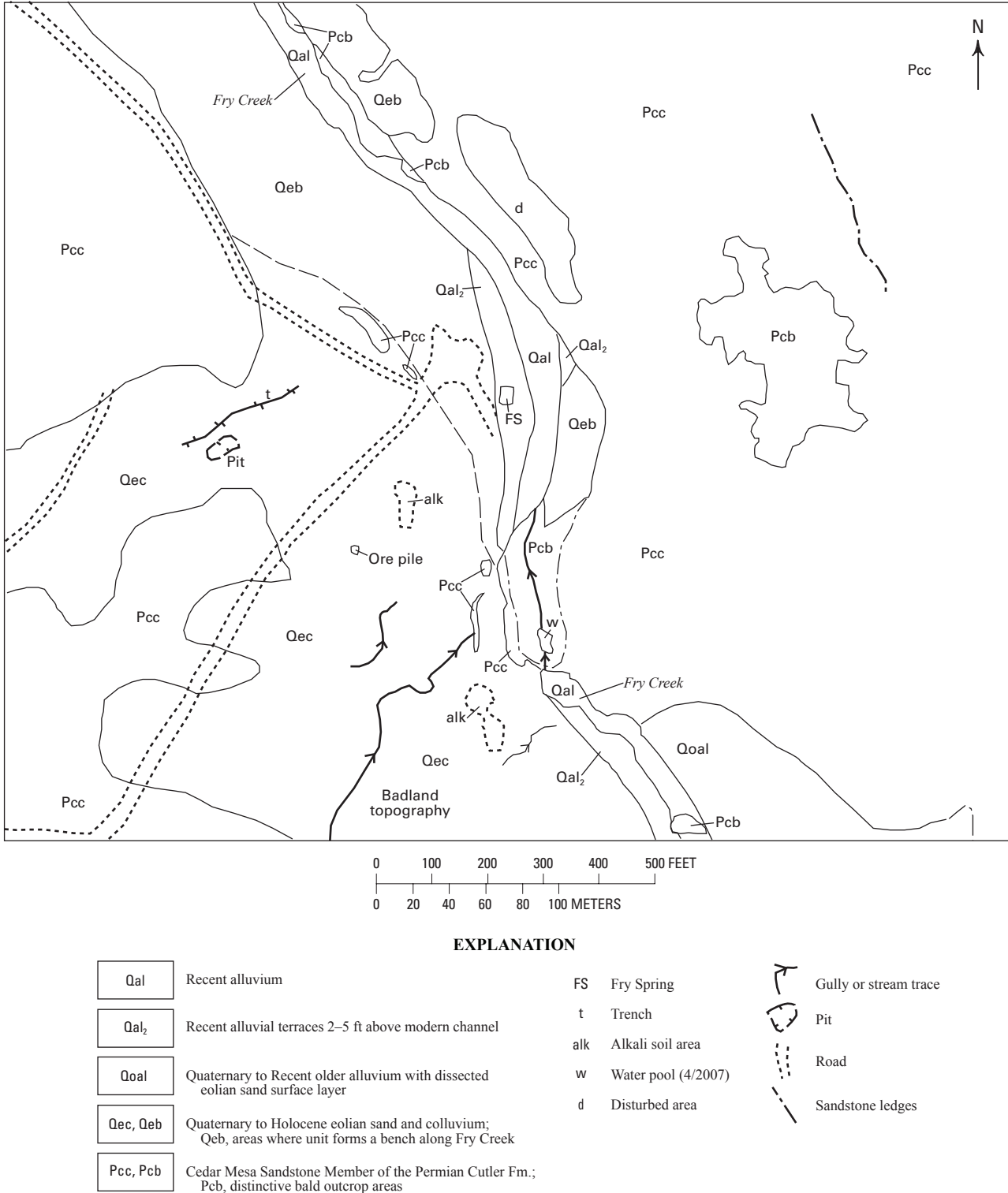


Figure 6. Geologic map of the Fry Spring area south of the Fry Canyon project site.

Overlying the sandstone are unconsolidated, reddish-brown, eolian sand and silty sand that contain lenses of colluvium composed largely of clasts of the Cedar Mesa sandstone mixed with reworked eolian sand (map unit Qec). Along the stream, these deposits overlie and intertongue with the basal gravels; they are also well exposed in the cutbank cliffs previously mentioned. The reddish-brown color contrasts with the white to gray colors of the Cedar Mesa sandstone. The map unit symbol Qec is used where these deposits occur in an upland setting, whereas Qeb is the symbol designation along the Fry Creek stream channel, where the unit forms a bench 3.7–5.5 m above the present-day stream channel (figs. 4–6). However, it should not be inferred that these deposits were stream deposited; rather, they were likely deposited by eolian and slope-wash processes without streamflow. In upland areas, Qec is mapped where it covers sandstone bedrock, but ledges of sandstone protrude through the sands in places, as shown in figures 4–6. The exposed maximum thickness of Qec is about 4.6 m, which is in the large mapped area of Qec west of Fry Creek in the southern part of figure 6. Along some gully exposures in this area, thin lenses of alluvium are present in Qec. Also in this area, Qec contains patches of alkali soils (“alk,” fig. 6), which are coated with surface salts (probably sulfate salts) and characterized by low, hummocky topography that resembles badlands (marked in fig. 6).

Alluvium has been deposited along most of the length of the active Fry Creek stream channel (Qal in figs. 4–6), except where sandstone bedrock is exposed. The alluvium is composed of sand to coarse, sandy, boulder gravel. Some sandstone boulders as large as 1.5–3.0 m across protrude through the alluvium. These boulders could be eroded from the very coarse boulder gravel layers present locally or from the local sandstone bedrock exposures. Clasts in the active alluvium are representative of most of the units exposed in the local drainage basin.

At a distance of 0.6–1.5 m above the active channel are low stream terraces subjected periodically to flooding (Qal₂, figs. 4–6). Higher stream terraces, such as the one near the cottonwood tree on the eastern edge of figure 4, have eolian sand deposited on them. Another stream terrace, in the southeastern part of figure 6, has a thick, gently dissected eolian sand covering the alluvium that is mapped as older alluvium (Qoal, fig. 6); it is distinguished from unit Qal₂ immediately west of the creek by being topographically higher and from unit Qeb 120–165 m to the north because the surface of the stream terrace is much lower and less dissected than the bench underlain by Qeb. It seems likely that floodwaters have seldom swept across this stream terrace. Another area of Qoal occurs on the west side of Fry Creek north of the ranch (fig. 4). It lies topographically about 3 m above an adjacent stream terrace underlain by Qal₂.

Eolian sand units (Qe), mapped separately in four areas in figure 4, do not contain interbedded colluvium lenses in the limited exposures examined by the author, and in one area there are small dune features.

Cross Sections—Geologic Relations and Interpretations

In order to better understand potential storage and pathways of movement of contaminated groundwater at the site, three cross sections (locations shown in fig. 5) were constructed: (1) one is oriented northeast, extending from the east corner of the berm of pond 6 along the berm between ponds 4 and 5 (through drill holes FC-5 and FC-8) and across Fry Creek to the exposed sandstone slope on the northeast side of the creek (*A–A'*, fig. 7); (2) a second extends nearly due north along a deeply eroded road trace that drops to the creek level at the north corner of the disturbed area and continues across the creek to bedrock on the north side (*B–B'*, fig. 8); and (3) a third extends north-south across the stream terrace abreast of the cottonwood tree and on across the creek (*C–C'*, fig. 9).

Cross section *A–A'* (fig. 7) shows that a 5.5-m-thick section of unconsolidated sediment underlies the approximately 4.3-m-high bench adjacent to Fry Creek. From nearby exposures and lithologic descriptions of well cuttings, this sediment appears to consist of tailings of varying thickness related to uranium operations, undisturbed eolian sand and colluvium deposited on the bench, and basal coarse gravels. As such, the two drill holes (FC-5, FC-8) define a paleochannel that is broader and deeper than the modern channel of Fry Creek (fig. 7). The limits of this paleochannel are considered to be the steep sandstone slope on the northeast side of the line of section and the sandstone ledges on the southwest side (shown hypothetically to the southwest of drill hole FC-8). The section in drill hole FC-5 contains more gravel than that observed in FC-8, indicating that the older stream channels tended to favor the northeast side of the valley, as they do now. The tailings and the underlying sand and gravel contaminated by leachate from the tailings and uranium- and copper-rich effluent placed in the ponds likely serves as a source for leachable uranium above the water table, a zone for temporary storage of uraniumiferous groundwater, and a pathway for movement of contaminated groundwater. The gravels may have high transmissivity.

Cross section *B–B'* (fig. 8) portrays vertical sections of surficial sediments exposed in a road cut and in a 3.7-m-high cutbank adjacent to the south side of the stream channel. No drill holes have been located at this site. In these places, three layers of gravel and boulder gravel are exposed; however, the upper layer of gravel appears to be partly eroded and the voids filled with eolian sand and colluvium. Eolian sand and colluvium also form the uppermost layers exposed in the cutbank. A sandstone ledge is exposed just below the road surface, about 12.2 m from the edge of the stream channel; however, well-rounded fluvial gravel laps onto the bedrock surface as much as 26 m from the edge of the modern stream channel. These older gravels may be present beneath the bench at the project site, but they were undetected in the drill holes studied by the authors.

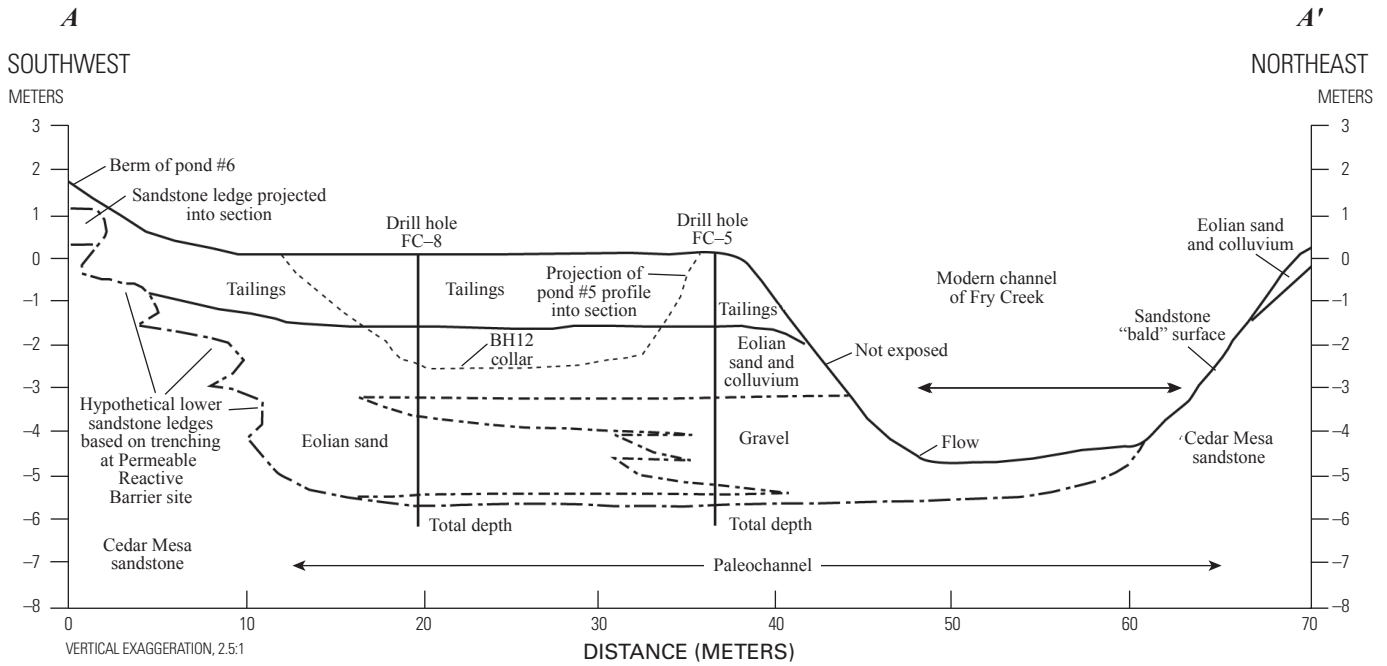


Figure 7. Cross section A-A' across the modern stream channel of Fry Creek and the bench to the south, at the position of the berm between ponds 4 and 5. See figure 5 for the line of section. Geochemical data for well FC-8 are in table 3. Datum for the cross section is the collar elevation of drill hole FC-8.

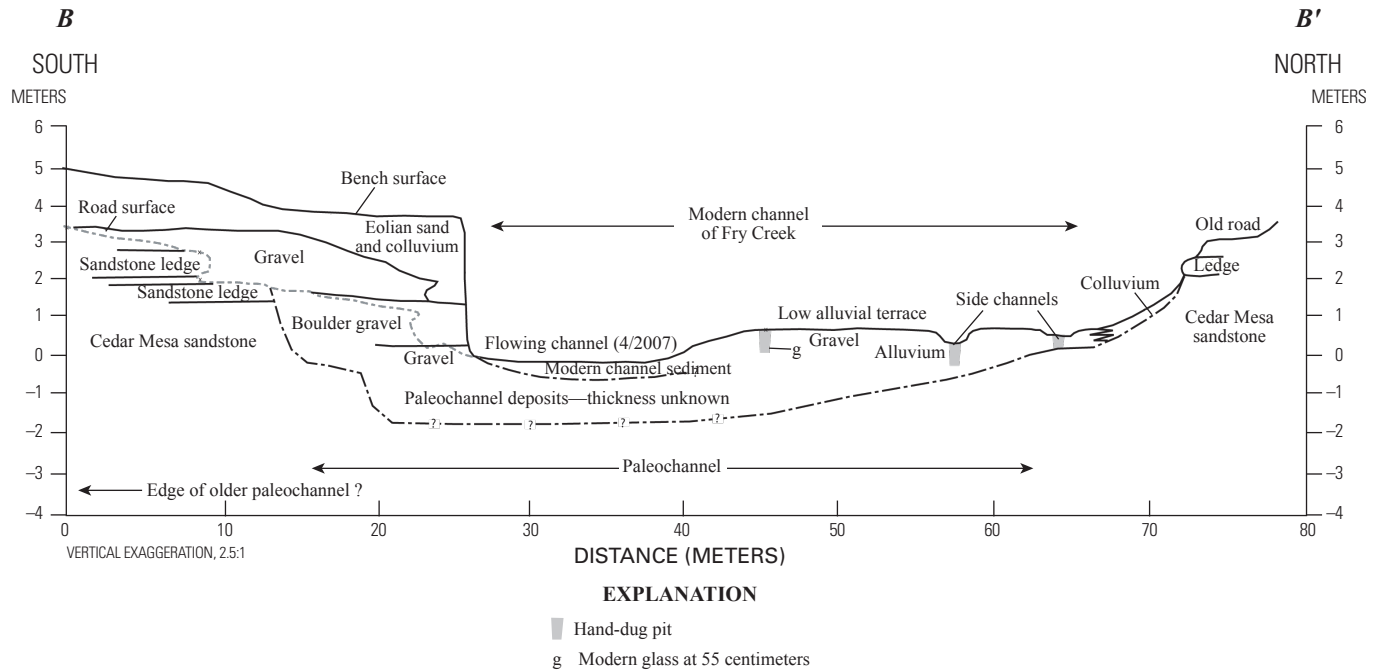


Figure 8. Cross section B-B' across the valley floor of Fry Creek north of the Fry Canyon project site at the location of a washed-out road. See figure 5 for location of section. Datum is the surface of the flowing channel.

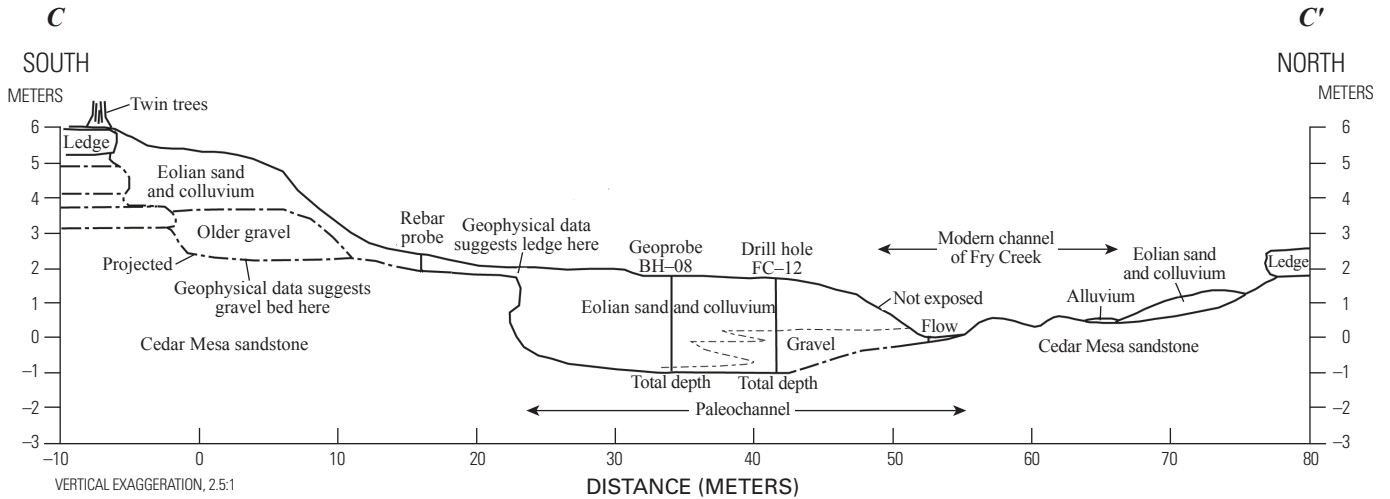


Figure 9. Cross section C–C' across the valley floor of Fry Creek at the location of the cottonwood tree well field. See figure 5 for location of section. Geochemical data for well FC–12 are in table 3. Datum is the surface of the flowing channel.

The depth of the valley fill beneath the exposed section and stream bottom is unknown. Four drives of rebar into the bottom of the modern channel went to refusal at 25–50 cm, but these depths are thought to represent the tops of large boulders (rather than bedrock) possibly at the top of older alluvium, such as that exposed at the base of the adjacent 3.7-m-high cutbank.

The relations described above indicate that the modern channel probably overlies much of the paleochannel, which presently may be carrying groundwater in the subsurface. The possible limits of this water-bearing paleochannel would extend from the sandstone ledge exposed at the bottom of the road cut south of the modern channel to the small hand-dug pit north of the modern channel that contacted bedrock below one of the side channels (see horizontal arrow, fig. 8). The thickness of the paleochannel sediments below the modern stream surface is not known.

Cross section C–C' (fig. 9) extends north from two prominent cedar trees perched on a thinly covered sandstone ledge through Geoprobe hole BH–08 and drill hole FC–12, across the narrow channel of Fry Creek, and up thinly covered sandstone bedrock to a sandstone ledge at the north end. The stream flows at the south edge of a bedrock exposure that probably defines the north edge of a paleochannel. The modern channel seems limited to the north by thin alluvium perched on bedrock and an adjacent eolian sand and colluvium deposit (see arrows in fig. 9). Drill holes BH–08 and FC–12 penetrated 2.7 m of sediment, which places some constraints on the width of the central part of the paleochannel. A rebar probe along the cross section went to refusal at a depth of 48 cm (fig. 9). If this represents the bedrock contact, the south edge of the paleochannel lies north of that location. A resistivity survey along this cross section (described in the following section) indicates that the position of south

edge of the channel is as shown in figure 9. The lithologic log for FC–12 shows 1.5 m of sand then 1.2 m of gravel and sand. The lithologic log for hole BH–08 was not available, but based on the driller's comments, most of the section is eolian sand and colluvium with thin fluvial gravels at the base as portrayed in figure 9. An area of high-standing sediment lies between the position of the rebar probe and the two cedar trees, forming a bench. Pebbles and cobbles lie at the toe of the slope. Geophysical data (discussed in the following section) indicate that a modestly thick section of damp sediment, herein interpreted as gravel, underlies this bench as shown in figure 9. This body of gravel may be correlative with the older gravels shown in the cross section in figure 8. Both bodies of gravel are at about the same height above the present-day stream channel.

In this location, the modern channel and the paleochannel overlap only slightly. The width of the paleochannel is reasonably well constrained by drill-hole and geophysical data. Water analyses from the monitoring wells in this stream terrace area show significant contamination from the project site.

Direct-Current Resistivity Survey

Four direct-current (dc) resistivity surveys were completed in the study area. All four lines were designed to delineate the possible subsurface extent of the paleochannel that parallels the modern stream channel and may underlie the adjacent stream terraces. Line FC–1 (fig. 10) was located in an area of monitoring wells near a cottonwood tree, a local landmark on the bank of Fry Canyon Creek, 200–300 m northwest of the uranium tailings ponds (see fig. 3 for location of the geophysical survey line). Line FC–3 (figs. 11, 3) started about

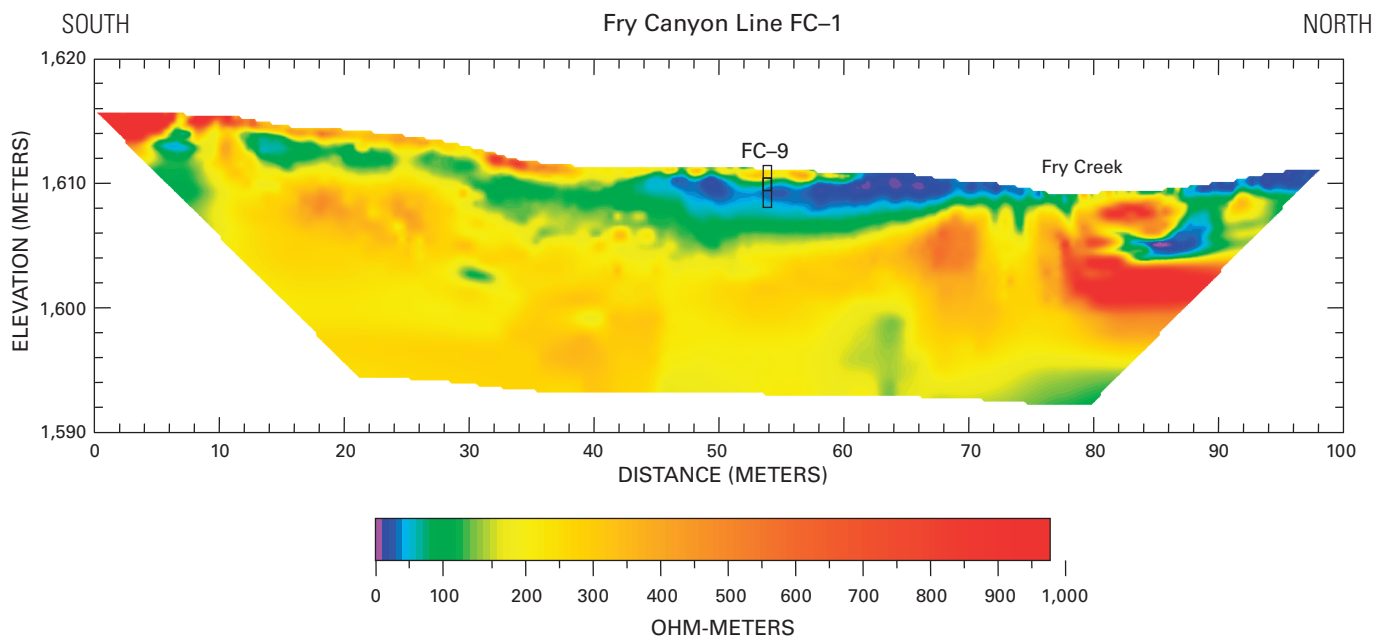


Figure 10. Direct-current resistivity profile for Fry Canyon line FC-1. See figure 3 for location. The location of monitoring well FC-9 is shown. The bar is 3 meters long. Specific conductivity data for well FC-9 are in table 2. See section “Direct-Current Resistivity Survey” for key to colors.

16 m north and 2 m west of the origin of line FC-1, diverged to the west and extended only to the edge of the creek. This line parallels geologic cross section C-C' (fig. 9) and extends from the -20 ft position to the 190-ft position on that section. Lines FC-1 and 3 have well data that show alluvium/bedrock contacts and thus provide some “ground truth” for interpreting the resistivity profiles. Line FC-2 (figs. 12, 3) extends from the modern stream channel across a terraced area between the cottonwood tree to the southeast and the ranch and barn complex to the northwest. Line FC-4 (figs. 13, 3) is located north of the ranch and barn complex in another terraced sector of the stream. There was no drill-hole control along these latter two lines.

Interpretation

The profiles show resistivity as a function of depth along each survey line. The resistive (low-conductivity) features seen in the profiles (red and orange features) generally represent dry materials, such as dry surface sediment and low-porosity bedrock. Low-resistivity (high-conductivity) features (purple and blue) generally represent wet and saline materials, such as wet sediment and groundwater in the alluvium. Moderately resistive features (green and yellow) generally represent alluvium or bedrock having a low moisture content and groundwater having a low TDS concentration. It is important to note that the horizontal and vertical scales vary from plot to plot. The horizontal scale of each profile was maximized for a page-size plot. The vertical scales are exaggerated for better anomaly resolution with depth.

Line FC-1

The purpose of line FC-1 (fig. 10) was to image the subsurface across the valley floor of Fry Creek between bedrock exposures on the south side of the creek and bedrock exposures on the north side. As noted, this line runs through an area of monitoring wells adjacent to a large cottonwood tree. Geologic and geochemical data for these wells provide ground truth information for interpreting the geophysical data and the evidence that groundwater in the sand and gravel present here is contaminated. The line is 100 m long and runs south to north roughly perpendicular to the creek valley. Important surface features to note include exposed bedrock near the start of the line at 0 m. Between 12 m and 30 m is a high, sloping bench surface separated by a steep slope between 30 m and 38 m from a lower stream terrace surface that extends to about 68 m. Streamflow and bedrock exposures extend from 75 m to 84 m. The creek runs between 78 and 79.5 m. Thin, saline, wet alluvium covers the bedrock from 88 m to near the end of the line. Monitoring well FC-9 is located at 52 m. Wet sediment, with surficial white salt crystals, is located at 74 m and between 82 and 84 m. Bedrock ledges crop out adjacent to 100 m.

The resistive zone at 0–6 m (fig. 10) is caused by the dry bedrock seen outcropping at the start of the line. A small, conductive, vertically oriented anomaly, located at 6–8 m and extending nearly to the surface, may represent a fractured bedrock zone with higher water and clay content. A thin, resistive surface layer, between 6 and 60 m, is caused by a dry layer of surficial sediment. The resistive material at depth in this interval (1,610-m elevation in the south part and 1,605-m elevation

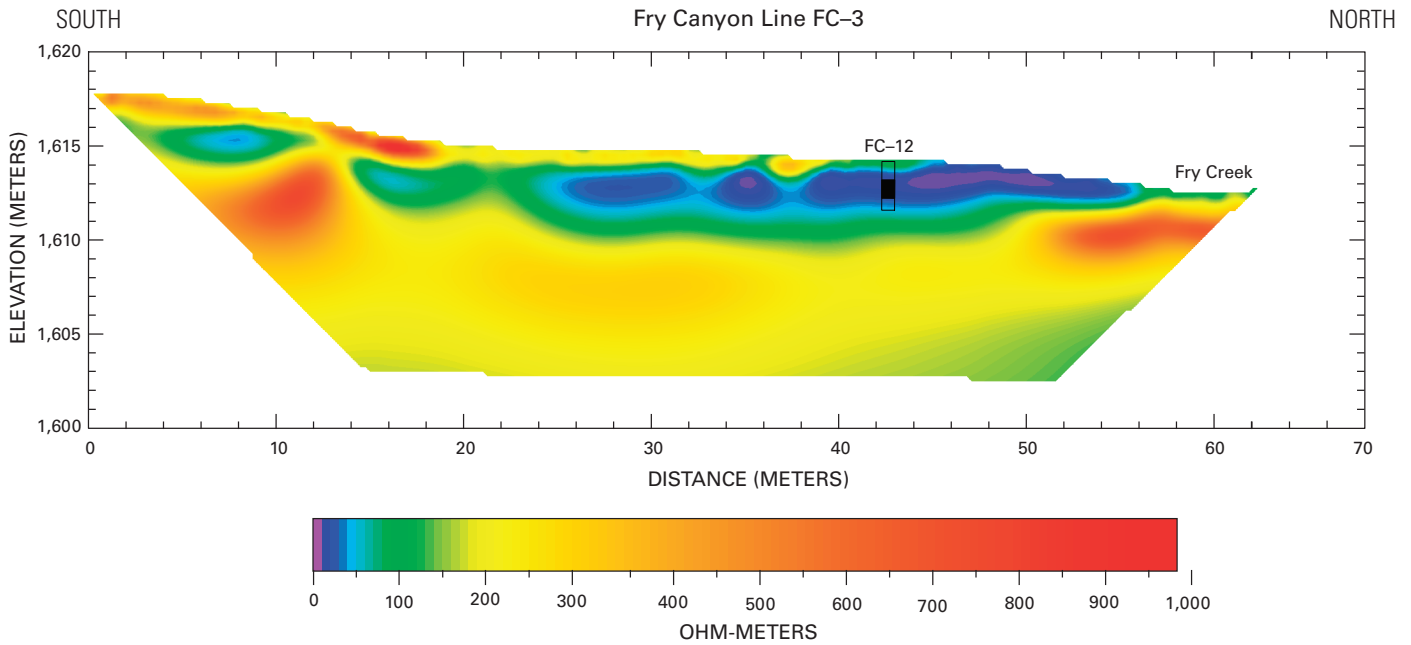


Figure 11. Direct-current resistivity profile for Fry Canyon line FC-3. See figure 3 for location. The location of monitoring well FC-12 is shown. The bar is 3 meters long. Specific conductivity data for well FC-12 are in table 2. See section “Direct-Current Resistivity Survey” for key to colors.

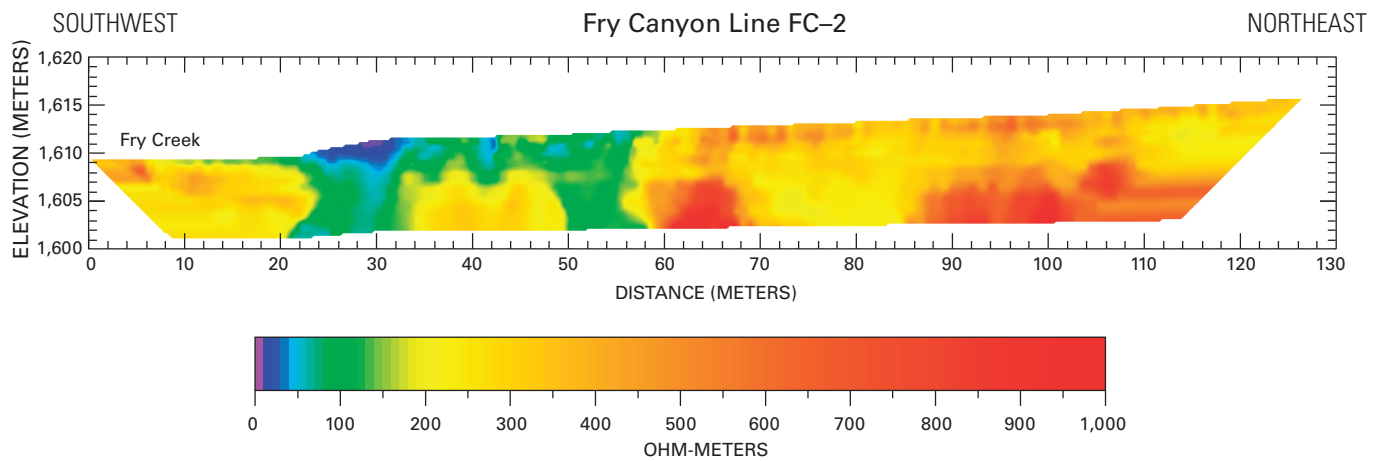


Figure 12. Direct-current resistivity profile for Fry Canyon line FC-2. See figure 3 for location. See section “Direct-Current Resistivity Survey” for key to colors.

in the north part) is low-porosity bedrock having a low moisture content. Between these two resistive layers, between 12 and 44 m, is a moderately conductive zone. There seem to be two sections to this zone. The conductive zone between 12 and 30 m is physically higher than the sector between 30 m and 42 m, as is the surface topography. This layer that extends from 12 to 30 m along the profile may represent damp, slightly saline sediment filling an older, high-standing channel. This part of geophysical profile FC-1 is contiguous to the

cross section in figure 9 and the associated geophysical profile FC-3, which are interpreted to show a high-standing gravel bed in a similar position.

The northern portion of this moderately conductive zone, extending from 30 to 42 m, appears to be underlain by bedrock. A rebar probe was driven into the ground to the west of this line, and a Geoprobe hole was driven into the ground to the east of this line. Both went to refusal on hard sandstone at depths of 0.3–0.6 m at a position equivalent to the 38-m mark

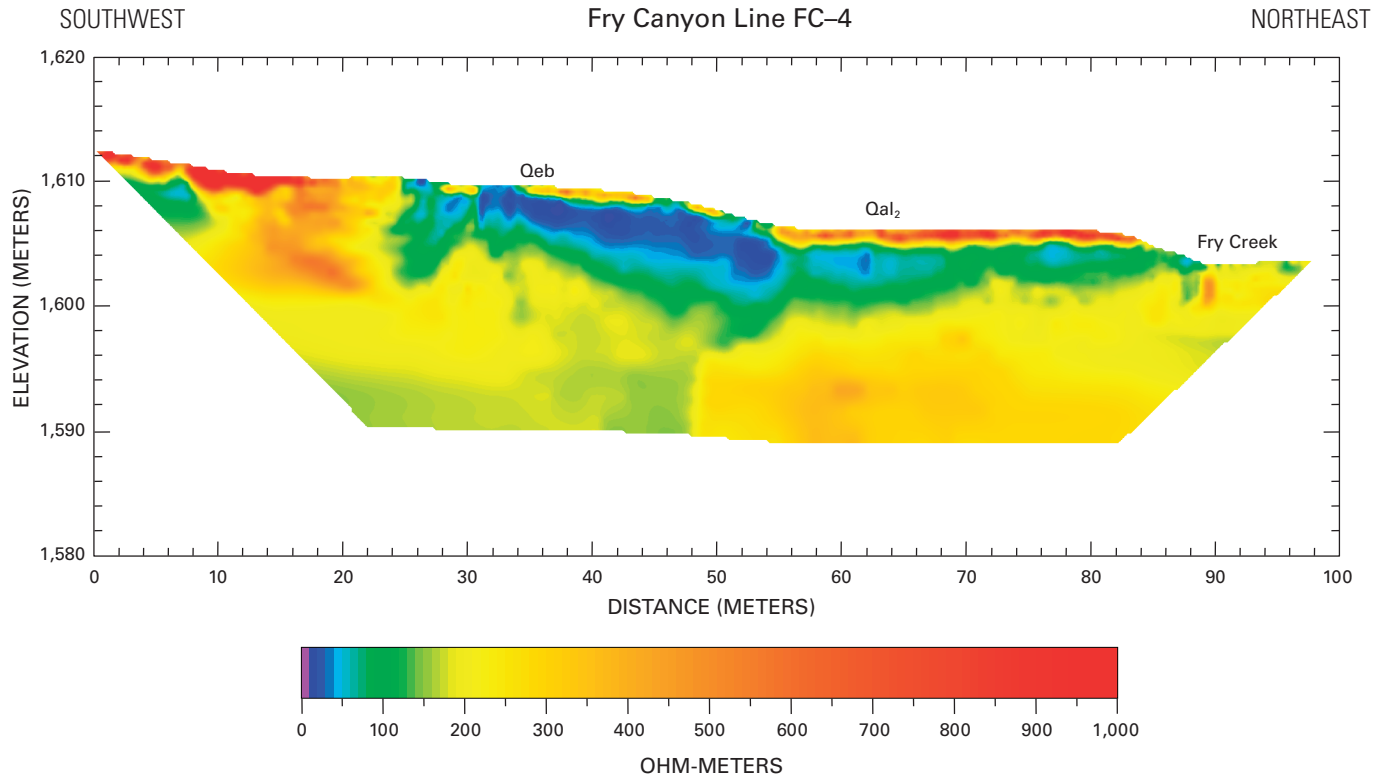


Figure 13. Direct-current resistivity profile for Fry Canyon line FC-4. See figure 3 for location. See section “Direct-Current Resistivity Survey” for key to colors.

along line FC-1. This moderately conductive zone between 30 and 42 m may represent (1) an inversion artifact produced by poor data coverage (see following discussion for FC-3); (2) moist bedrock composed of thin sandstone, siltstone, and mudstone (upstream from Fry Spring, springs were observed issuing from thin siltstone and mudstone layers beneath an overhanging ledge of sandstone); or (3) a paleochannel filled with sandstone boulders and other sediment, the rebar and Geoprobe both fortuitously contacting large sandstone boulders seen elsewhere.

A wide, very low resistivity zone is located between 45 and 76 m. It extends to the streambank adjacent to the surface flow in the modern stream. This shallow conductive zone is as much as 6 m thick, and the upper, more conductive part (1–3 m deep) is interpreted as water-bearing and saline sediment filling a buried bedrock channel. Monitoring well FC-9 (shown by a 3-m-long bar) is located within this conductive zone, and bedrock was contacted at a depth of 3.05 m with saturated sediment in the 0.6–1 m interval above bedrock (Brent Lewis, Bureau of Land Management, unpublished drill-hole logs). The data in the profile do not seem to discriminate between the damp to wet unsaturated zone and the 0.6–1-m-thick saturated zone, suggesting that salinity in the unsaturated zone and groundwater blur the distinction. The more modest conductive zone below (3–6 m deep) may represent bedrock partly saturated with saline water.

From 62 to 76 m along the profile very low resistivity extends to the surface, suggesting that saline sediment dominates the unsaturated zone. White, damp, salt deposits on alluvial sediments were observed on the surface in this area, indicating that the shallow groundwater has relatively high TDS and that the unsaturated zone has significant salt accumulations. Evapotranspiration concentrates the salts in the near-surface sediments, resulting in a low-resistivity, though unsaturated, surface layer.

At the location of well FC-9 the resistivity profile shows values of 50–70 ohm-m (pale blue) at a depth of 3 m, which likely represents the sediment/bedrock contact given the drill-hole intercept. This drill-hole intercept and portions of this conductive anomaly are below the elevation of the current stream channel where bedrock is exposed, suggesting that a paleochannel is present here.

A resistive near-surface zone is located between 78 and 86 m. This resistive feature probably represents the shallow bedrock exposed adjacent to the stream along the modern channel. Being located immediately below the current stream channel, but having a high resistivity, indicates the bedrock has a low porosity and is relatively unfractured at this location. The small, subhorizontal conductive anomaly, centered at 85 m and extending as much as 6 m below the surface, probably represents a fractured bedrock zone containing high-TDS water. A long, wide, sinuous fracture is present in the

exposed bedrock at this location. A surface layer of conductive alluvial sediment with saline crusts extends from 87 m to the end of the traverse near the base of bedrock ledges. At depths below 6 m the high resistivity indicates that the bedrock is not porous or fractured.

Line FC-3

Line FC-3 (fig. 11) is also located near the cottonwood tree (fig. 3). The purpose of line FC-3 was to provide subsurface information along the geologic cross section shown in figure 9. The line is 64 m long, runs subparallel to line FC-1, and has similar features. The line starts at two large juniper bushes, which are on the north edge of a thinly covered bedrock ledge; this line then crosses the valley onto bedrock exposed just north of the flowing stream (from the -20 to the +180 ft positions in the cross section in fig. 9). Important surface features to note in profile FC-3 include exposed bedrock 2 m south of station 0 and from 60 to 64 m. A small patch of rounded (fluvial?) cobbles lies at the surface at the toe of the slope at about 20 m. A rebar probe was driven into the ground at 22 m. Geoprobe hole BH-08 is located at 35 m (not shown). Well FC-12 is located at 42 m (a 3-m-long bar marks the location). Bedrock intercept data provide information important to interpreting the geophysical data along line FC-3. Damp sediment with surficial white salt crystals is located on the streambank between 53 and 55 m. The stream is located at 58 m.

From 0 to 40 m, a thin resistive layer is located along the surface and is produced by dry, sandy sediment (fig. 11). Immediately below this resistive layer, the ground becomes more conductive, indicating an increase in moisture or salt content. A moderately conductive anomaly extending from 4 to 12 m suggests the presence of shallow, damp, somewhat saline sediment, possibly representing a perched gravel bed similar to that noted in the southern part of line FC-1. The rounded cobbles observed at the surface at 20 m may have been weathered out of such a gravel bed. The conductive zone located between 14 and 20 m at a depth to 4 m, is similar to the zone seen in FC-1. This interval occurs in a similar position but with less resolution due to poor data coverage (see Appendix 2, fig. 26). The rebar probe at 22 m intercepted hard sandstone at 0.5 m. This anomaly is poorly constrained and cannot be interpreted as a real subsurface feature without further information. At depth below 4 m the section becomes resistive, indicating bedrock having a low porosity and low moisture content.

A low resistivity zone is located between 24 and 56 m. This shallow zone extends from about 1 to 4.5 m deep, and the upper, more conductive part from 1 to 3 m likely includes 0.6–1 m of water-bearing sediment and overlying saline unsaturated-zone sediment. The relatively low resistivity suggests the saturated sediments contain conductive water. Like profile FC-1, the shape and depth of the anomaly suggest the presence of a sediment-filled bedrock channel. Geoprobe hole BH-08 and monitoring well FC-12 are located within this conductive zone. Both wells indicate bedrock at a depth of 3.05 m (Brent

Lewis, Bureau of Land Management, unpublished drill-hole logs). At both locations and similarly to the intercept in profile FC-1, the profile shows resistivity values of 50–70 ohm-m at a depth of 3 m, which probably represents the sediment/bedrock contact.

The surface is very conductive between 46 and 56 m. Surface salt deposits were observed within this area, indicating shallow groundwater with high TDS and concentration of salts in the unsaturated zone by evapotranspiration.

The thin, modestly conductive surface layer between 56 m and the end of the line is produced by wet sediment in the current stream channel. Here, the sediment is very thin with salt crusts overlying resistive bedrock. The high resistivity of the underlying bedrock suggests it has low porosity and is relatively unfractured at this location.

Line FC-2

Line FC-2 (fig. 12) is located approximately 200 m downstream from line FC-1 (fig. 3). The purpose of line FC-2 was to image the subsurface below the modern stream channel and a broad, very gently sloping stream bench on the east bank of the creek. The line is 128 m long and strikes approximately N.40°E. across the creek valley. The line runs from low bedrock exposures on the southwest edge of the wide, modern stream channel up onto the bench. Bedrock cliffs occur to the southwest of this line. Bedrock outcrops are observed approximately 15 m beyond the northeast end of the line. Important surface features to note include exposed bedrock in the streambed from 0 to 6 m. The creek flows between 9.5 and 11 m. Thin, wet sediment in the streambed lies on bedrock and is covered with white salt crystals between 6 and 24 m. The streambank is covered with white salt crystals from 24 to 26 m.

The southwest half of line FC-2 is considerably more conductive than the northeast half (fig. 12). The abrupt change in the near-surface resistivity observed at 58 m is interpreted as moist to wet sediment overlying saturated and unsaturated bedrock to the southwest, in contact with dry sediment over dry bedrock to the northeast. The relatively thick conductive zone located between 22 and 58 m, from the surface to a depth of about 4 m, is interpreted, in part, as wet fluvial sediment filling a broad paleochannel in the bedrock. The deep conductive zones, from 20 and 34 m and from 50 and 58 m, are interpreted as bedrock having greater porosities, possibly due to fracture zones, and containing increased amounts of groundwater. The relatively low resistivity of these zones suggests groundwater having relatively high TDS. The depth of the paleochannel is difficult to pick because of the apparent bedrock fracture zones, but it may be a meter or so below the modern stream channel.

The most conductive feature on the profile is located between 24 and 32 m. This shallow conductive zone is located on the sloping bank of the stream and the adjacent stream terrace edge, between the current channel and the stream terrace.

The zone is 3–4 m thick, and is partly coincident with an area covered with white salt crystals. This conductive zone probably results from wet surface sediment having a high salt content. The surficial salt deposits suggest evapotranspiration and accumulation of salts in the unsaturated zone derived from the shallow groundwater.

The resistive surface, from 0 to 8 m, is produced by exposed bedrock in the stream channel. The thin surface conductive zone, from 10 to 22 m, is produced by the layer of wet sediment overlying resistive bedrock in the streambed. Based on the observed surficial salt crystals in this area, the water in the sediment is probably quite conductive due to the presence of dissolved salts. Resistive bedrock underlies the southwestern end of the line from 0– to 22 m. The modern stream channel is located over this part of the line; the resistive nature of the bedrock suggests it is composed of impermeable, unfractured sandstone having a low water content. Only relatively minor, tight fractures were noted in bedrock exposures.

Northeast of 58 m, the character of the profile becomes relatively resistive. Here, the surface is slightly more resistive, to a depth of 2–3 m, than the underlying material. The resistive surface layer is interpreted as dry sediment overlying bedrock having a low water content. The resistive features at depth represent dry or impermeable sandstone having little or no groundwater. The more conductive zones at depth (that is, 70–85 m) are probably bedrock zones having slightly higher porosities. There seems to be no evidence in this profile for a high-standing gravel-filled paleochannel; however, if such a channel were completely dry, it may not be distinguishable from dry surface sediment or bedrock.

Line FC–4

Line FC–4 (fig. 13) is located approximately 400 m downstream from line FC–2 (fig. 3). The purpose of line FC–4 was to help define the west edge of the bedrock channel, which is covered by surface sediment on a two-level stream terrace. The line is 100 m long and strikes approximately N. 50° E. The line begins on high ground with bedrock outcrops about 80 m west of the stream and runs downhill, across a gently sloping high stream terrace, an essentially flat lower stream terrace, then across the stream and onto bedrock in the modern stream channel. This line is located north of the area mapped in figure 4, but the features mapped extend to the position of the profile.

Important surface features to note include thin dirt cover over bedrock from 0 to 19 m. The line follows a shallow gully from 10 to 19 m. The upper stream terrace is located between 25 and 54 m (including the toe of the stream terrace). The lower stream terrace extends from 56 to 84 m and the streambank from 84 to 88 m. The stream is located between 90 and 92 m. Wet surface sediment is located between 90 and 93 m. Wet sediment, with surficial white salt crystals, overlying bedrock is located between 93 and 102 m, beyond the profile.

In line FC–4 the highly resistive surface layer, located between 0 and 20 m, results from dry bedrock (fig. 13). The increase in conductivity with depth suggests that the water content increases. A small conductive anomaly, located at 8 m, may represent a fractured bedrock zone with higher water content.

A relatively thick, sloping conductive zone lies between 26 and 54 m and corresponds with a mapped older stream terrace just upvalley (Qoal in fig. 4). The upper part of the conductive zone (that part less than 50–70 ohm-m in resistivity) is interpreted as wet to saturated saline sediment overlying bedrock, based on the 50–70-ohm-m values used to define a wet sediment/bedrock contact in FC–1 and FC–3. A thin resistive layer, produced by dry surficial sediment, covers much of this conductive feature. Much of this conductive anomaly is well above the modern stream channel. Therefore, the water source is not the stream; the source probably is buried bedrock springs and fractures recharged from the high ground to the west. We are uncertain if this is a sediment-filled channel equivalent to the higher channel suggested by the high-standing gravel in figure 9 and the possible high-standing channel in profiles FC–1 and FC–3.

The abrupt resistivity contrast at depth (represented by juxtaposed pale green and pale orange colors), located at 48 m and extending from 1,590 to 1,596-m elevation, is an inversion artifact produced by poor data coverage (see Appendix 2 and fig. 28). This vertical feature is poorly constrained and should not be interpreted as a real subsurface feature.

The part of the line located between 54 and 84 m crosses a wide, flat stream terrace. The thin surface resistive layer is dry surface sediment, noticeably thicker than the layer covering the conductive layer to the west. The conductive zone immediately beneath is interpreted as wet, somewhat saline sediment. This conductive zone, which overlies relatively resistive bedrock at depth, is partly below the modern stream-channel elevation and may represent sediment filling a broad channel in bedrock. This channel would seem to be the lower paleochannel traceable through the three previous profiles, here about 30 m wide. Extremely low resistivity (<50 ohm-m) saline sediment on the streambank between the creek and the lower terrace, seen in other profiles, is not seen here. From 90 to 100 m, the very thin surface conductive layer is produced by wet, saline sediment in the modern stream channel. The underlying resistive zone is the shallow bedrock, which is widely exposed on the flat stream channel bottom. Surficial salt deposits observed here on the thin alluvium indicate that the shallow groundwater has high concentrations of TDS.

Structure

Dips of the bedrock in the mapped areas were difficult to determine, but generally they were about 1 degree to the west. The geologic and regional structure contour map of Thaden and others (1964, plate 1) showed that strikes of the section in Fry Canyon were about N. 10° W. and dips were about 1.3° W.

Fractures in the Cedar Mesa sandstone are not abundant but may form local pathways for the migration of contaminants into bedrock as indicated by the resistivity profiles previously described. Fractures were observed in exposures of bedrock on natural balds, along the stream channel, and in areas disturbed by bulldozing. Most fractures are thin, sinuous, and of limited lateral extent. One fracture zone located west of, and downslope from, heap leach piles is as much as 25 centimeters wide and contains crushed sandstone; however, this zone could not be traced laterally because of cover. Fractures along the modern stream channel have been opened up by erosional processes and are generally filled with alluvium. Depths of any of these filled fractures cannot be determined from surface exposures. It seems likely that similar open fractures may be associated with the

trace of the paleochannel in the subsurface, and such fractures may be pathways for movement of contaminated water into the bedrock, as suggested by the resistivity profiles.

General Chemical Character of Water

Waters sampled in this study are of circumneutral to slightly alkaline pH (6.75–8.65) and moderate specific conductance (1,200–2,800 microsiemens per centimeter (μS/cm), table 2). Total dissolved solids (calculated) range from 820 to 2,800 mg/L, which indicates slightly saline waters (Hem, 1985). Seeps and springs are slightly less saline than surface waters and downgradient well waters, which in turn are slightly less saline than plume wells on the Fry Canyon project

Table 2. Chemical and isotopic composition of surface water, seeps, springs, and wells, Fry Canyon, Utah.

[NAD27 CONUS, North American Datum 1927 Continental United States; Spec. cond., specific conductance; TDS, total dissolved solids; μS/cm, microsiemens per centimeter; °C, degrees Celsius; mg/L, milligram per liter; μg/L, microgram per liter; km, kilometer; ft, feet; Est., estimated; <, less than]

Sample ID	Location notes	(NAD27 CONUS/12S)		Est. accuracy (ft)	Longitude (west)	Latitude (north)	Fry Creek (km)	Fry Creek (miles)
		GPS-Easting	GPS-Northing					
07FC-W1	Upstream where surface flow first occurs	576811	4162450	18	110.130	37.608	0	0
07FC-W2	Seep pool in side channel adjacent to Qal-2	576858	4162615	17	110.129	37.609	0.193	0.12
07FC-W3	Seep pool in side channel adjacent to Qal-2	576846	4162920	14	110.129	37.612	0.499	0.31
07FC-W4	Seep from under overhanging sandstone ledge, near Fry Spring	576758	4163041	19	110.130	37.613	0.66	0.41
07FC-W5	Spring from side wash, near Fry Spring	576747	4163057	40	110.130	37.613	0.676	0.42
07FC-W6	Fry Spring—north edge of pool	576745	4163142	29	110.130	37.614	0.74	off channel at 0.46
07FC-W7	Surface flow of stream, just upstream from Fry Spring	576768	4163132	18	110.130	37.614	0.74	0.46
07FC-W8	Seep pool at base of salt cedar adjacent to berm of Pit #2	576544	4163439	18	110.133	37.617	1.127	0.7
07FC-W9	Surface water adjacent to cottonwood tree well field	576192	4163610	14	110.137	37.618	1.545	0.96
07FC-W10	Surface flow of stream downvalley from the ranch site	575859	4164122	18	110.140	37.623	2.462	1.53
07FC-W11	Stagnant pool in small slot canyon downvalley from ranch	575355	4164905	16	110.146	37.630	3.541	2.2
07FC-W12	Stagnant pool, slot canyon just upstream from bridge	575120	4165436	20	110.149	37.635	4.41	2.74 (bridge at 2.80)
07FC-W13	Cottonwood tree well field—Well FC9	576195	4163582	20	110.137	37.618		
07FC-W14	Cottonwood tree well field—Well FC12	576187	4163590	23	110.137	37.618		
07FC-W15	Contaminant plume—Well FC7	576436	4163498	28	110.134	37.617		
07FC-W16	Contaminant plume—Well FC4	576453	4163495	19	110.134	37.617		
07FC-W17	Contaminant plume—Well FC8	576464	4163464	20	110.134	37.617		
07FC-W18	Contaminant plume—Well FC3	576434	4163508	0.6	110.134	37.617		
07FC-W19	Fry Spring—Well FC1	576727	4163155	(SAIC) 0.6	110.131	37.614		
07FC-W20	Cottonwood tree well field—Well FC11	576203	4163587	(SAIC) 16	110.137	37.618		

Table 2. Chemical and isotopic composition of surface water, seeps, springs, and wells, Fry Canyon, Utah.—Continued

NAD27 CONUS, North American Datum 1927 Continental United States; Spec. cond., specific conductance; TDS, total dissolved solids; $\mu\text{S}/\text{cm}$, microsiemens per centimeter; $^{\circ}\text{C}$, degrees Celsius; mg/L, milligram per liter; $\mu\text{g}/\text{L}$, microgram per liter; km, kilometer; ft, feet; Est., estimated; <, less than]

Sample ID	Temp. $^{\circ}\text{C}$	pH	Spec. cond. ($\mu\text{S}/\text{cm}$)	TDS mg/L (calc.)	SiO_2 (mg/L)	Na (mg/L)	K (mg/L)	Ca (mg/L)	Mg (mg/L)	Fe (mg/L)	Cl (mg/L)	SO_4 (mg/L)	HCO_3 (mg/L)
07FC-W1	15	8.30	2,400	1,438.58	14.9	453	9.6	35.8	45.0	<0.05	135	428	675
07FC-W2	15	8.55	1,450	964.79	12.7	266	5.8	36.6	55.4	<0.05	68	201	675
07FC-W3	17	7.60	1,200	822.15	16.1	232	4.6	35.5	35.9	<0.05	62	184	545
07FC-W4	10	7.90	1,200	907.34	12.3	260	5.7	39.8	34.4	<0.05	75	220	555
07FC-W5	14	7.65	1,450	964.68	15.9	272	5.4	38.6	40.7	<0.05	84	251	555
07FC-W6	15	8.05	1,400	937.47	10.4	262	5.7	38.5	41.5	<0.05	77	233	570
07FC-W7	18	8.15	1,200	843.99	14.6	238	5.3	28.5	36.1	<0.05	70	210	520
07FC-W8	11	7.85	1,700	1,152.84	15.7	352	7.7	41.9	35.3	<0.05	101	266	710
07FC-W9	20	8.00	1,500	1,000.01	12.9	281	7.2	40.1	40.3	<0.05	83	283	540
07FC-W10	25	8.50	1,750	1,150.32	4.6	353	14.7	23.4	41.2	<0.05	109	361	505
07FC-W11	21	8.45	2,000	1,316.20	4.3	395	13.9	32.0	45.3	<0.05	131	436	535
07FC-W12	15	8.65	1,950	1,275.04	3.4	387	13.5	27.8	41.8	<0.05	130	433	493
07FC-W13	11	7.55	1,400	1,042.14	11.3	273	4.5	47.4	39.9	<0.05	90	329	525
07FC-W14	11	7.40	1,400	1,080.72	11.9	297	5.5	48.4	42.1	<0.05	93	324	550
07FC-W15	13	7.00	2,800	2,801.40	7.8	26.5	9.7	580	184	<0.05	0.5	1,906	193
07FC-W16	12	7.10	1,600	1,155.80	10.2	277	5.1	67.3	58.6	<0.05	92	366	590
07FC-W17	13	6.75	1,900	1,483.67	8.5	251	5.0	133	101	<0.05	93	600	610
07FC-W18	12	7.10	1,980	1,390.17	9.0	262	5.6	139	64.6	<0.05	92	554	555
07FC-W19	12	7.60	1,490	962.31	17.6	267	4.4	37.8	41.3	<0.05	82	255	558
07FC-W20	10	7.50	1,650	1,033.08	11.7	279	4.7	46.6	40.5	<0.05	87	317	525

site. Sample W15 collected from the center of the contaminant plume stands out because it is approximately twice as saline (2,800 mg/L) as any other water sample. Based on the milliequivalent per liter (meq/L) concentrations of major cations and anions, most sampled waters are of the Na-Mg- HCO_3 or Na-Mg- HCO_3 - SO_4 chemical types. An important exception is well water W15, which is Ca-Mg- SO_4 water with relatively minor amounts of bicarbonate, chloride, and sodium compared to the other waters (fig. 14). Contrasting chemistry of contaminant plume water and local water was noted earlier (Naftz and others, 2000) and indicates that plume water chemistry is variably affected by calcium and sulfate derived from the heap leach piles. Other dissolved anions (fluoride, nitrate, phosphate) were not measured but are of probable low concentration based on the close agreement (± 3 percent) of calculated cation-anion balances for the waters using only bicarbonate, sulfate, and chloride.

The seeps, springs, and surface waters are noteworthy for generally elevated concentrations of dissolved uranium (34–256 $\mu\text{g}/\text{L}$) when compared to the U.S. Environmental Protection Agency drinking-water standard of 30 $\mu\text{g}/\text{L}$ (U.S. Environmental Protection Agency, 2001). This suite includes seven samples collected upstream from the Fry Canyon site (W1–W7; 44–58 $\mu\text{g}/\text{L}$) and is presumed to represent local baseline values. High natural baseline concentrations of dissolved uranium in oxygenated surface water and groundwater are expected in this setting that includes numerous local uranium mines, prospects, and radioactive anomalies (Thaden and others, 1964). However, aerosol sand, silt, dust, and salts from close and distant sources can also contribute major, minor, and

trace elements to soils and subjacent groundwater. Thick sections of eolian sediment are present here. The high concentrations of dissolved uranium (380–578 $\mu\text{g}/\text{L}$) in three monitoring wells (W13, 14, 20) are clearly anomalous compared to baseline values and are highly suggestive of variable contamination from the Fry Canyon project site.

In contrast to uranium, concentrations of dissolved copper are generally less than 20 $\mu\text{g}/\text{L}$ —the result of solubility control by insoluble copper hydroxides and carbonates or strong sorptive uptake by ferric oxyhydroxides (Hem, 1985). One exception is plume well W17, which contained 200 $\mu\text{g}/\text{L}$ copper and anomalous concentrations of manganese (1,460 $\mu\text{g}/\text{L}$) and zinc (590 $\mu\text{g}/\text{L}$) (table 2). This well water was identified as metal-rich in previous sampling (Wilkowski and others, 2002). Water collected from this well contained abundant suspended oxyhydroxides that are efficient sorbents for trace metals and probably are not completely removed during filtration through a 0.45- μm filter membrane.

Excluding the equivocal data from plume well W17, dissolved concentrations of most other measured trace elements (manganese excluded) were less variable than uranium and were less obviously elevated in the remaining plume wells (W15, W16, W18) compared to other water samples. Concentrations also generally fell below comparative benchmarks such as drinking-water standards or aquatic-life standards (U.S. Environmental Protection Agency, 2006a, 2006b). A few arsenic concentrations slightly exceeded the current drinking-water standard of 10 $\mu\text{g}/\text{L}$. A few concentrations of selenium and copper slightly exceeded a value of 5 $\mu\text{g}/\text{L}$, which may be harmful to some forms of aquatic life.

Table 2.—Continued

Sample ID	As (µg/L)	B (µg/L)	Ba (µg/L)	Cu (µg/L)	Li (µg/L)	Mn (µg/L)	Mo (µg/L)	Ni (µg/L)	Se (µg/L)	Sr (µg/L)	V (µg/L)	Zn (µg/L)	U (µg/L)	²³⁴ U/ ²³⁸ U Activity ratio	δ ³⁴ S (permil)
07FC-W1	12	130	97	9	198	1	42	4	5	950	5	3	58	1.229±.011	-5.4
07FC-W2	8	92	97	16	150	2	23	4	3	1,210	6	3	45	1.089±.005	-2.4
07FC-W3	5	72	50	7	127	0	19	3	3	990	3	17	47	1.279±.005	-3.1
07FC-W4	5	75	50	5	128	0	26	2	6	990	6	2	58	1.223±.007	-3.2
07FC-W5	4	82	49	4	127	0	25	2	11	1,090	9	2	58	1.271±.001	-3.4
07FC-W6	3	77	41	4	128	0	19	2	5	1,080	6	3	58	1.283±.003	-3.3
07FC-W7	7	84	85	5	134	1	23	2	4	910	5	1	44	1.270±.002	-3.3
07FC-W8	13	85	149	8	157	3	16	5	4	960	6	2	34	1.150±.005	1.8
07FC-W9	6	88	92	8	140	1	24	3	5	1,020	7	3	152	1.064±.003	-2.8
07FC-W10	10	105	83	13	167	2	32	2	6	840	10	3	199	1.048±.003	-2.8
07FC-W11	10	94	111	15	191	3	37	3	6	1,010	9	18	255	1.050±.005	-2.7
07FC-W12	10	98	110	16	182	2	37	3	6	880	10	7	256	1.052±.001	-2.9
07FC-W13	3	69	26	8	142	245	32	4	3	920	1	3	578	0.985±.002	-3.4
07FC-W14	2	76	24	7	141	112	28	6	5	1,040	2	7	380	1.012±.004	-3.5
07FC-W15	1	63	15	13	177	2	17	25	17	3,100	0	25	18,700	0.939±.005	-13.3
07FC-W16	2	83	25	7	148	40	4	17	8	1,340	0	18	770	0.954±.006	-3.1
07FC-W17	2	104	16	200	226	1,460	3	79	4	1,070	0	590	2,160	0.932±.005	-1.2
07FC-W18	2	73	28	6	157	210	3	13	4	1,470	0	6	2,070	0.930±.003	-1.5
07FC-W19	3	81	30	4	125	2	20	2	11	1,130	6	2	70	1.282±.004	-4.0
07FC-W20	3	70	28	4	126	372	29	5	3	950	1	4	429	0.985±.004	-3.4

Other trace elements sought but below 10 µg/L include Ag, Al, Be, Bi, Cd, Cr, Pb, Sb, and Tl.

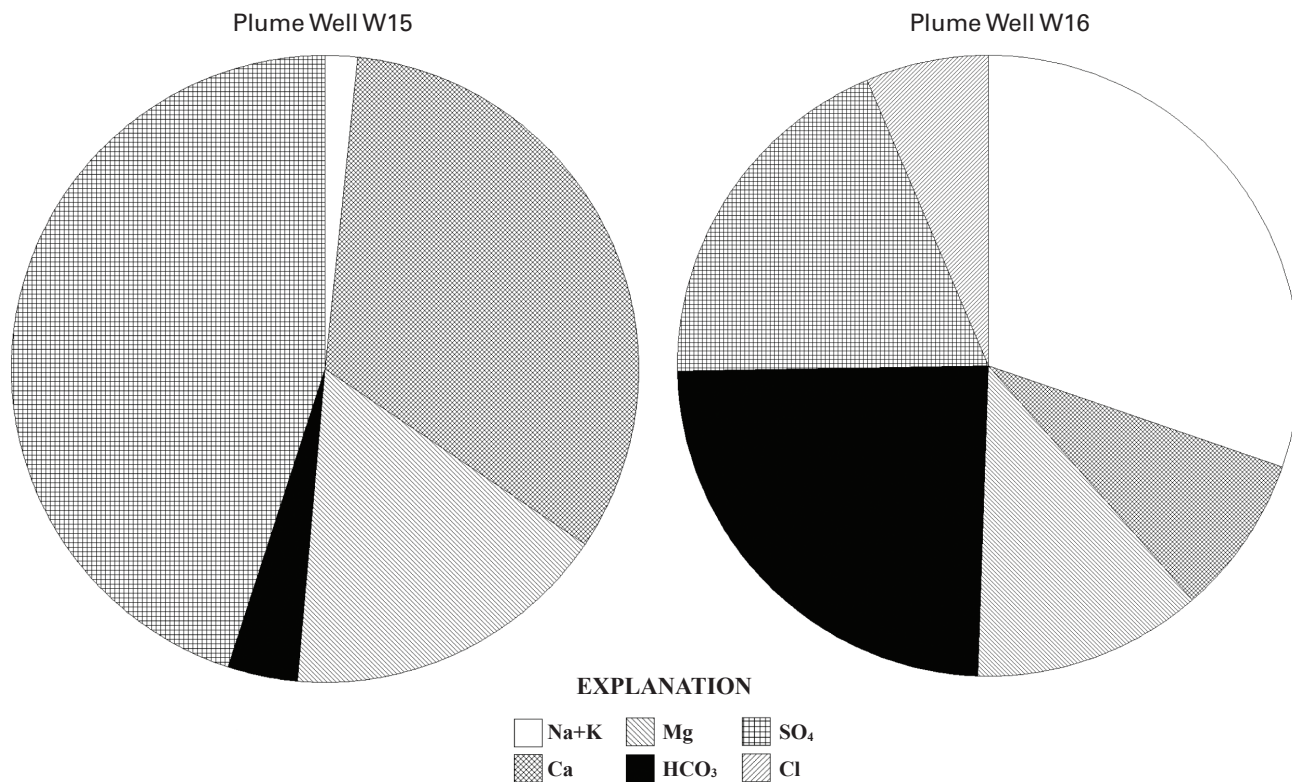


Figure 14. Pie diagrams showing the relative percentages of major cations and anions (on a milliequivalent basis) in well W15 from the center of the contaminant plume and well W16, which is more representative of other contaminated water samples collected in this study.

Aqueous Geochemistry of Uranium

In oxygen-bearing surface waters and shallow groundwaters of this study, uranium is oxidized to soluble U(VI) and occurs as a variety of soluble species, depending upon pH. Under acid-oxidizing conditions, U(VI) occurs primarily as the uranyl cation (UO_2^{+2}), whereas under alkaline-oxidizing conditions of this study, U(VI) forms highly stable anionic complexes with dissolved carbonate that enhance its solubility (Langmuir, 1978). Speciation of dissolved U(VI) in each of the sampled waters was calculated using the computer code PHREEQC (Parkhurst, 1995), utilizing the WATEQ4F thermodynamic database (Ball and Nordstrom, 1991). For these calculations an oxidation potential (Eh) of +0.4 volt was used to simulate an oxygenated aqueous environment. For most waters of this study, uranyl tricarbonate [$\text{UO}_2(\text{CO}_3)_3^{-4}$] complex is dominant, and uranyl dicarbonate [$\text{UO}_2(\text{CO}_3)_2^{-2}$] is of minor to submajor importance (fig. 15). Uranyl ion also forms a complex with dissolved phosphate at circumneutral pH (Langmuir, 1978), but very low concentrations of dissolved phosphate in most natural waters probably limit the contribution of this complex.

The PHREEQC computer code also permits calculation of the degree of saturation of waters with respect to a variety of minerals, including uranium minerals. Results for each mineral are expressed as a saturation index defined as the logarithm of the ratio of the ion activity product (IAP) divided by the equilibrium solubility product (K_{sp}). These

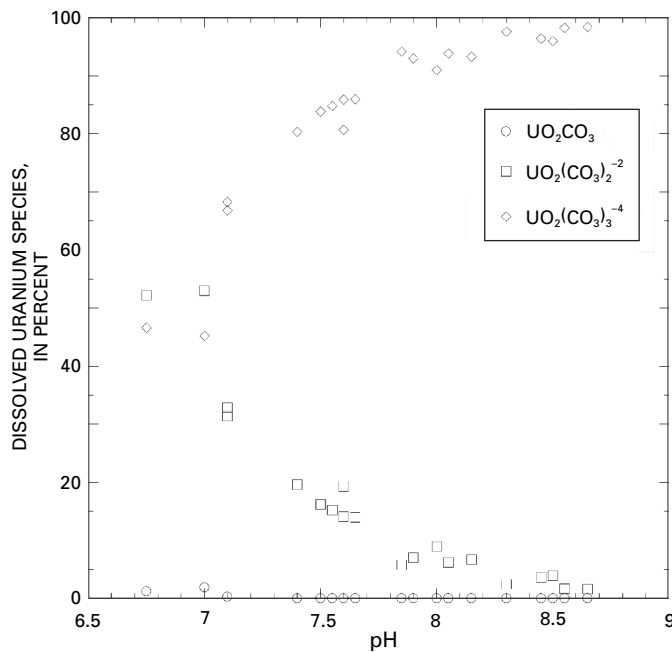


Figure 15. Plot showing the relative abundance of major dissolved U(VI) species as a function of pH in waters of this study. Calculations were assigned an oxidizing Eh of +0.4 volt.

thermodynamic-based calculations assume mineral/solution equilibria and, because reaction kinetics are not considered, are best interpreted as potentials for mineral dissolution (undersaturated condition) or mineral precipitation (oversaturated condition). Accuracy depends on the quality of the chemical analyses and the accuracy and internal consistency of the thermodynamic database. A value of zero for the saturation index indicates equilibrium saturation, positive values indicate oversaturation, and negative values undersaturation. Results for the sampled waters (fig. 16) indicate slight undersaturation or larger oversaturation with respect to quartz, calcite, dolomite, and ferrihydrite and undersaturation with gypsum and representative copper minerals malachite [$\text{Cu}_2(\text{CO}_3)(\text{OH})_2$] and tenorite [CuO]. All waters are highly undersaturated with the reduced U(IV) minerals uraninite (UO_2) and coffinite [$\text{U}(\text{SiO}_4)_{1-x}(\text{OH})_{4x}$] and also with all U(VI) minerals in the PHREEQC database. Additional saturation indices for uranyl vanadate minerals were calculated using the thermodynamic database attached to the MINTEQA2 computer code (Allison and others, 1991). The U(VI) minerals include carnotite [$\text{K}_2(\text{UO}_2)_2(\text{VO}_4)_2 \cdot 3\text{H}_2\text{O}$], schoepite [$(\text{UO}_2)_4\text{O}(\text{OH})_6 \cdot 6\text{H}_2\text{O}$], rutherfordine [$(\text{UO}_2)_3\text{CO}_3$], tyuyamunite [$\text{Ca}(\text{UO}_2)_2(\text{VO}_4)_2 \cdot 5-8\text{H}_2\text{O}$], and uranophane [$\text{Ca}(\text{UO}_2)_2(\text{SiO}_3)_2(\text{OH})_2 \cdot 5\text{H}_2\text{O}$]. U(VI) minerals show closest approach to saturation in the most uranium-rich water from plume well W15 but are still an order of magnitude undersaturated, considering the logarithmic scale of figure 16.

At the concentration of dissolved uranium in these waters (and most natural waters), uranium solubility is most likely limited by sorptive processes rather than uranium mineral saturation (Langmuir, 1978). The most likely sorbents for uranium at the site are ubiquitous secondary iron oxides that coat many grains and impart a reddish color to local sediments. Sorptive uptake of dissolved uranium by these phases is inhibited, however, by the formation of highly stable carbonate complexes, by the alkaline pH, and by local evaporative conditions that can produce elevated salinity in pore waters (Hsi and Langmuir, 1985; Ho and Miller, 1986).

Considering the above discussion, the oxic near-surface environment surrounding the Fry Canyon project site offers little to impede the solubility and mobility of uranium. Minimal sequestration of dissolved U(VI) in the local environment dictates use of permeable reactive barriers that employ efficient sorbents or surface complexers of U(VI), or chemical reductants that convert U(VI) to highly insoluble U(IV) (Wilkowski and others, 2002). Calculations with PHREEQC indicated that precipitation of uraninite from uranium-rich water of well W15 composition requires Eh values lower than 0.15 volt. Eh values well below 0.15 volt are reported in pore waters of the PRB-containing reductant of zero-valent iron (Wilkowski and others, 2002).

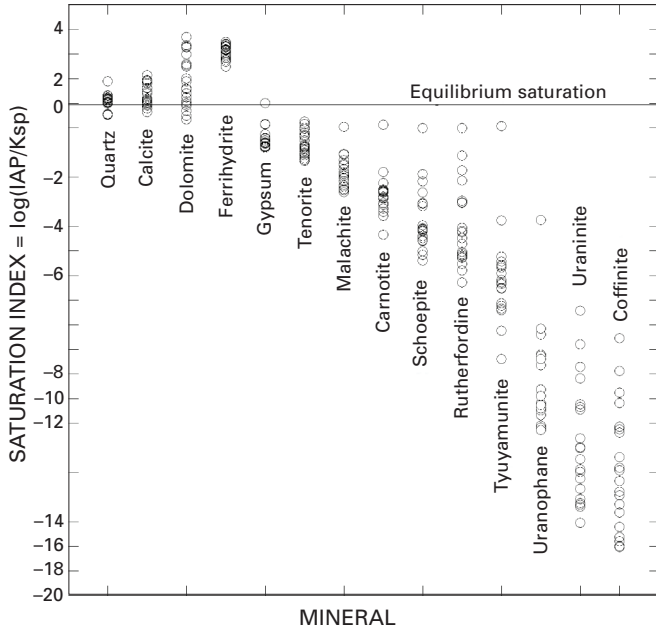


Figure 16. Plot showing degree of saturation of sampled waters with respect to a variety of minerals, including uranium minerals. An Eh of +0.4 volt was assigned to these oxygen-bearing waters. Most waters are undersaturated with respect to most minerals, as indicated by plotted positions below the equilibrium saturation reference line. IAP, ion activity product; Ksp, equilibrium saturation product.

Spatial Distribution of Dissolved Uranium

Dissolved uranium concentrations in seeps and surface waters of Fry Creek ranged from 40 to 60 µg/L upstream from the Fry Canyon project site but increased abruptly to 150 µg/L at the first stream location (W9) sampled downstream from the site (fig. 17). Dissolved uranium concentrations continued to increase in a downstream direction and plateau at values of approximately 250 µg/L. These observations indicate that site-derived uranium is contributing to uranium load in the stream and that uranium stored in downstream sediments may be an additional source of dissolved uranium. Uranium isotopes (see subsequent discussion) can be used to identify contributions of natural and site-derived uranium in these more downstream waters.

An additional possibility is that downstream concentrations of uranium from all sources are increased by evaporative concentration in places where surface flow is sluggish or where stream water infiltrates the shallow (less than 1 m) alluvium. This hypothesis is supported by the greater dissolved-solids content (approximately 30 percent) in downstream waters (table 2) and by observed efflorescent crusts of “white alkali” salts in dry or slightly moist portions of the

streambed (fig. 18). These salts are brought to the surface by capillary action during evaporation from a shallow water table and consist predominantly of highly soluble sodium sulfate and sodium-magnesium sulfates. Dissolution of these salts from stream sediments or local soils likely influences the major-ion chemistry of both surface water and shallow groundwater (table 2).

Uranium Isotopes

The ²³⁴U/²³⁸U activity ratios (AR) of seven baseline samples (W1–W7) collected upstream from the Fry Canyon project site had a mean value of 1.235±0.069 (table 2). Values of AR greater than the radioactive equilibrium value of 1.0 are common in surface waters and result from preferential leaching and decay-induced recoil of ²³⁴U during slow weathering of uranium-bearing rocks and minerals (Osmond and Cowart, 1976). In contrast, four stream waters collected downstream from the site (W9–W12) all have AR values in the narrow range of 1.048–1.064, suggesting that any added site-derived uranium had an AR value less than 1.05 (fig. 19). Persistence of this isotopic composition in downstream samples indicates that at the time of sampling, additional mixing with isotopically distinct sources of “natural” uranium of AR~1.2–1.3 was minimal.

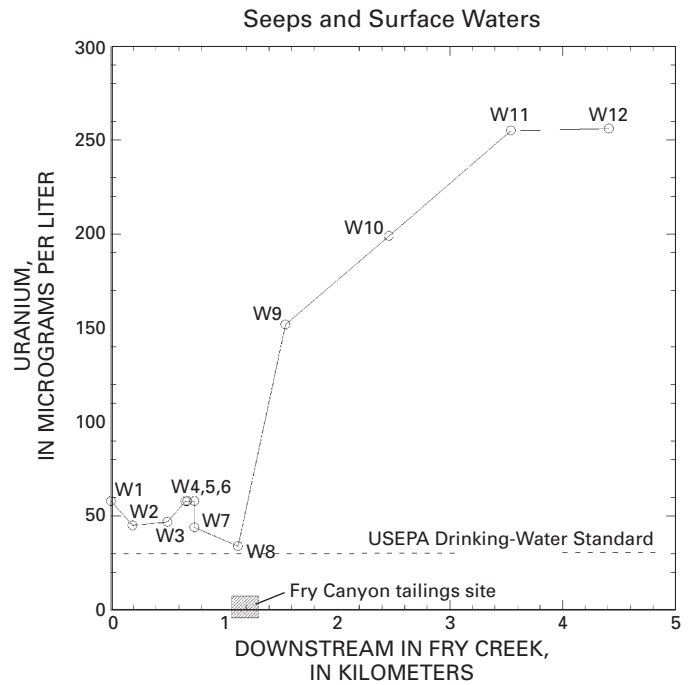


Figure 17. Plot of dissolved uranium concentration as a function of sampling-site location (fig. 2) along the main stem of Fry Creek. The location of the Fry Canyon project site is shown for reference as is the USEPA drinking-water standard of 30 micrograms per liter.



Figure 18. Photograph of view upstream from water-sampling site W1 in Fry Creek. Deposits of white sodium sulfate and sodium-magnesium sulfate salts form evaporative crusts in the dry streambed.

The four contaminant plume wells (W15–W18) had a mean AR of 0.939 ± 0.011 (table 2). Values of $AR < 1.0$ in the contaminant plume result from aggressive leaching of mined Cu-U ores and host rock by sulfuric acid in the heap-leach pile. Rapid and nearly quantitative removal of uranium minimizes fractionation of uranium isotopes and produces AR values in leachates that mimic AR values of the original ore/rock. A plot of AR compared to $1/U$ (fig. 20) indicates that three monitoring wells in the cottonwood well field (W13, 14, 20) located approximately 0.5 km downgradient from the Fry Canyon project site (fig. 2, table 2) have AR values that fall on a linear mixing trend line connecting the average AR of contaminant plume wells (0.939) and the AR for the upstream Fry Spring well (1.282). Site-derived uranium was expected in the monitoring wells considering their relatively high concentrations of dissolved uranium (380–578 $\mu\text{g/L}$, table 2). Simple isotope mass-balance calculations using the end member AR values cited previously indicate that approximately 78–87 percent of uranium in the monitoring wells is site-derived. Similar mixing proportions based on chemical mass balance can be calculated using assumed average uranium concentrations in the end members, but because uranium concentrations are more temporally variable than uranium isotopic ratios, the isotope-based approach is more robust. As remediation activities progress on the site, uranium isotopes will continue to indicate mixing proportions in these wells, even as concentrations decrease to near-baseline levels.

The four surface-water samples collected downstream from the Fry Canyon site also fall on the mixing trend line and indicate consistently high percentages (about 67 percent) of site-derived uranium. Horizontal scatter of these points about the mixing line is probably caused by evaporation that

affects uranium concentration but not isotopic composition. Likewise, predominantly horizontal scatter of most plotted values for upstream baseline samples indicates variable dilution of a composition similar to the Fry Spring well. One stream sample (W8) collected adjacent to the Fry Canyon project site plots to the right of the mixing line, indicating that it has too low a uranium concentration for its AR. This sample is a mixture of bank seepage from the site plus streamflow and was collected from stagnant water containing abundant organic debris. Some dissolved uranium may have been removed by local reducing conditions within the adjacent bank or in the streambed. In addition, complex organic compounds were used as frothing agents in processing ores at the site. Biodegraded remnants of these compounds occur in sediment in the pits and may be present in these waters and act as additional reductants.

Although not a major process affecting the sampled waters, chemical reduction of dissolved uranium has the same effect on plotted points as dilution; AR values remain effectively unchanged as uranium concentration decreases ($1/U$ increases). Pore waters within the zero-valent iron PRB should therefore plot within a broad horizontal field delimited in the vertical dimension by AR values similar to the contaminant plume wells. Mixing relationships between such pore waters of variable and low uranium concentration and local waters would generate a cloud of plotted points on the right half of figure 20.

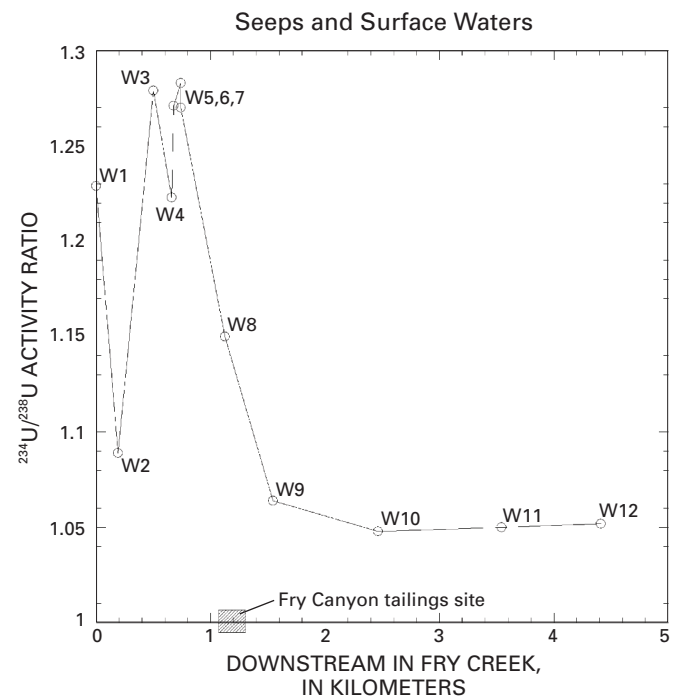


Figure 19. Plot of $^{234}\text{U}/^{238}\text{U}$ activity ratio (AR) of water as a function of sampling-site location (fig. 2) along the main stem of Fry Creek. The location of the Fry Canyon project site is shown for reference.

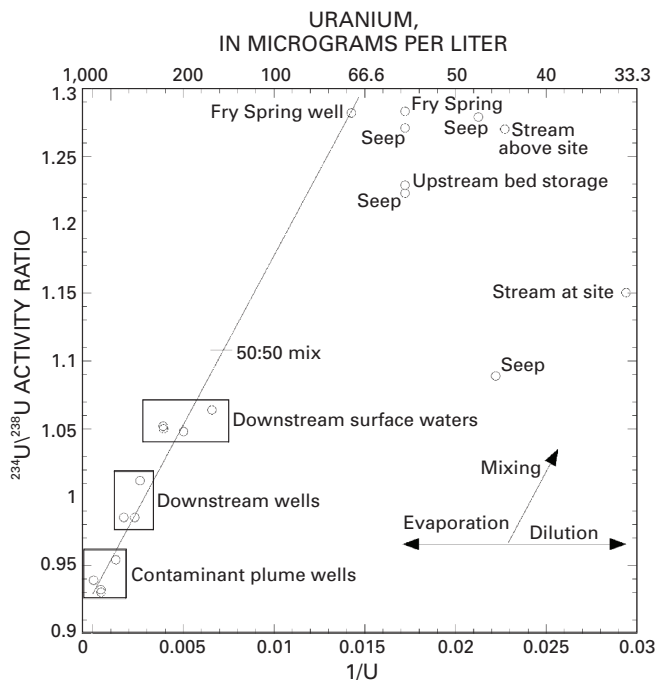


Figure 20. Plot of $^{234}\text{U}/^{238}\text{U}$ activity ratio (AR) compared to dissolved uranium concentration in waters of this study. AR values of low-uranium waters collected upstream from the Fry Canyon project site are greater than 1.0, whereas AR values of well waters from the uranium-rich contaminant plume are all less than 1.0. Most other sampled waters lie along a mixing line connecting these two end-member types.

Sulfur Isotopes

The sulfur isotopic composition ($\delta^{34}\text{S}$) of sulfate in most of the measured waters plots in the narrow range of -2.4 to -5.4 per mil (fig. 21). This range includes all of the upstream (baseline) waters (table 2) and indicates that at the time of sampling, dissolved sulfate in most of the measured waters was dominantly of natural origin. Local dissolved sulfate is derived by solution of sparingly soluble gypsum and more soluble “white alkali” salts in colluvium, alluvium, and eolianite. The original source of sulfur is sulfide minerals present in Paleozoic and Mesozoic sedimentary rocks that underlie the region and are exposed on mesas that provide topographic relief.

An important exception to sulfur isotopic uniformity is plume well W15, which has $\delta^{34}\text{S}$ of -13.3 per mil. This composition may represent another component of sulfate derived from the heap leach pile. Sources of sulfur in the heap-leach pile include sulfide and sulfate minerals in the various Cu-U ores transported to the site, and sulfur in the applied sulfuric acid. Other plume well waters of somewhat elevated dissolved sulfate concentration do not lie along a mixing trend line anchored by W15 (fig. 21). Instead, they trend in the opposite direction toward less negative $\delta^{34}\text{S}$ values. At times of higher

water levels, the plume wells near W15 may be more influenced by natural sulfate derived from the host stream terrace. The bench also hosts a series of ponds that were formerly settling ponds used in the uranium upgrading operations (figs. 3 and 5). Ponds were supplied with local sulfate-bearing water that underwent evaporative concentration and percolated into the underlying bench sediments. During drier periods when the contaminant plume is a bigger contributor to a thinner saturated zone, wells near W15 may be more influenced by heap-leach or tailings-derived sulfate (Naftz and others, 2006).

Another exception is stream water W8 collected adjacent to the Fry Canyon project site and exhibiting $\delta^{34}\text{S}$ of $+1.8$ per mil. This isotopically heavier composition could result from local sulfate-reducing conditions in the streambank or streambed that favor the lighter ^{32}S isotope and therefore enrich remaining dissolved sulfate in ^{34}S . Note that this same water had unusually low uranium concentration for its AR value, suggestive of chemical reduction of dissolved uranium.

Sulfur isotope measurements indicate two isotopically distinct sources of sulfate in plume wells, but this is not the case for dissolved uranium. The extremely large contrast in uranium concentration (about $400\times$) between the contaminant plume composition (W15) and natural waters produces a wider halo of dominant uranium contamination in the network of plume wells.

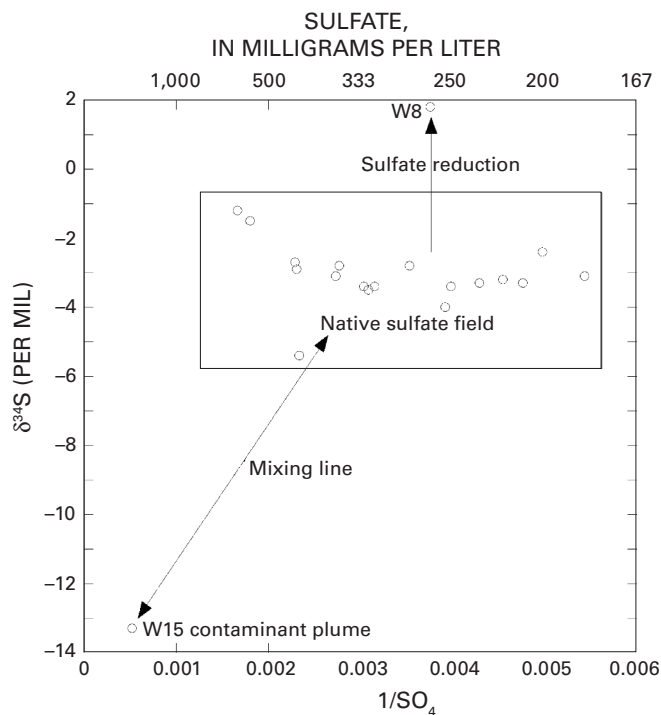


Figure 21. Plot of $\delta^{34}\text{S}$ of dissolved sulfate compared to dissolved sulfate concentration in waters of this study. Most waters plot in a narrow range of values that includes uncontaminated waters collected upstream from the Fry Canyon project site. Exceptions include chemically distinct, sulfate-rich water from the center of the contaminant plume (W15) and one stream water (W8) possibly affected by sulfate reduction.

Sediment Chemistry and Mineralogy

Two 60- to 120-mesh size fractions collected from the slope of tailings adjacent to Fry Creek (T1, T2, fig. 2, inset; also fig. 3) are obviously enriched in uranium (100×) and copper (130–180×) compared to the same size fraction from “baseline” stream sediment sample S1 (fig. 2, inset; table 3). Other trace elements showing lesser enrichments in tailings include lead (4×), zinc (10×), and arsenic (6–9×). Chemical indications of tailings contributions to sediments S2–S7 located downstream from the site are primarily based on enrichments compared to S1 and are most obvious for copper in S2 (2×), which is approximately 0.1 km downstream from the tailings (fig. 2). Smaller apparent enrichments (1.15–1.35×) of uranium, lead, and zinc in S2 are too small to confidently exceed (by 2 standard deviations) the mean of their concentrations in more downstream samples. Copper concentration in sample S5 (13.4 µg/g) is anomalously high compared to most of the sediment samples but not compared to S1. Concentrations in S7 are probably influenced by additional detritus contributed by tributary drainages to Fry Creek (fig. 2).

Sulfide grains in the magnetic fraction of tailings sample T1 identified under reflected light illumination (fig. 22A–F) were predominantly pale brassy yellow chalcopyrite [CuFeS₂], with lesser amounts of beige-white pyrite [FeS₂] and much rarer grains of peacock-blue bornite [Cu₃FeS₄] (fig. 22C). Pyrite is nonmagnetic, but magnetic properties could result from partial alteration to various secondary iron oxides (observed), formation of composite grains of pyrite with chalcopyrite (observed), or incorporation of some copper in the pyrite structure. Chalcopyrite and pyrite grains showed variable amounts of alteration to secondary iron oxides that coat grains, fill fractures, or replace original sulfide. In addition, many chalcopyrite grains showed uneven, pitted polishing surfaces perhaps caused by chalcopyrite growth as pore fillings around other, now-absent phases. The distinctive large and highly reflective grains of chalcopyrite constitute perhaps 10 percent of the grains in the magnetic concentrate from the tailings. A few grains in the T1 concentrate contained rounded forms of framboidal pyrite enclosed by non-reflective matrix that is probably partly degraded organic matter

(fig. 22B). Rare pale green grains or grain coatings observed under a binocular microscope in the T1 magnetic concentrate are probably fine-grained malachite [Cu₂(CO₃)(OH)₂] or azurite [Cu₃(CO₃)₂(OH)₂]. Specimens of these brightly colored copper minerals can be found at scattered locations throughout the Fry Canyon site.

The thin section of magnetic minerals from baseline sediment S1 contained numerous grains coated by, or altered to, secondary iron oxides that appear in various shades of gray, blue-gray, or blue-white under the immersion oil and reflected light illumination. Some of these grains may be former sulfide minerals of natural origin that have completely altered during their prolonged history of oxidative weathering, transport, and within-stream reworking. A few rare grains contained occasional tiny inclusions of relict pyrite of probable natural origin.

The most downstream sediment sample, S7, had no sulfide grains in thin section. The other magnetic mineral concentrates of sediment samples S2–S6 contained from 1–9 grains of tailings-derived sulfides in thin section. As expected, the number of tailings-derived sulfides in thin sections tended to decrease with increasing (downstream) distance from the tailings source [S2(9), S3(6), S4(2), S5(7), S6(1)], but limited sample size and rarity of target sulfide grains precludes strict quantitative comparisons. Temporal and spatial variations in stream-channel morphology influence flow patterns and can concentrate heavy minerals in small areas of streambed that may not be uniformly sampled. Sampling of such an area could explain the relatively large number of sulfide grains (7) in sample S5 (fig. 22G–K), collected approximately 1.3 km downstream from the tailings source.

Backscatter electron image and X-ray intensity maps for copper, iron, and sulfur generated by electron microprobe scans of thin section T1 (fig. 23) confirmed relatively abundant chalcopyrite (CuFeS₂) compared to pyrite (FeS₂) and also identified rare grains of a more copper-rich sulfide (bornite?). Other grains containing lower concentrations of copper probably are chalcopyrite, now variably altered to iron oxides. Many grains of low iron content seen on the iron map are other minerals coated by iron oxides.

Table 3. Concentrations of selected trace elements (µg/g) in the 60–120 mesh size fraction of tailings and stream sediments, Fry Canyon, Utah.

[µg/g, microgram per gram; **, probably enriched; *, possibly enriched]

Sample	Copper	Uranium	Lead	Zinc	Chromium	Vanadium	Arsenic	Manganese
Tailings T1	1,890	89	16	104	5.7	11.3	22.7	166
Tailings T2	2,690	124	21	104	5.5	12.5	29.6	135
Sed 1 (baseline)	14.5	1.0	5.3	11.2	5.2	11.4	3.9	526
Sed 2	27.2**	1.3*	6.1*	14.8*	5.1	14.9	4.0	231
Sed 3	11.9	1.1	5.5	10.7	5.2	14.3	3.2	243
Sed 4	8.4	1.1	5.1	10.1	4.0	11.1	2.3	254
Sed 5	13.4*	1.1	5.5	13.7	5.6	14.5	3.1	250
Sed 6	9.2	1.2	5.9	13.3	4.8	12.6	2.4	262
Sed 7	3.0	0.9	5.4	12.7	5.5	11.7	2.2	222

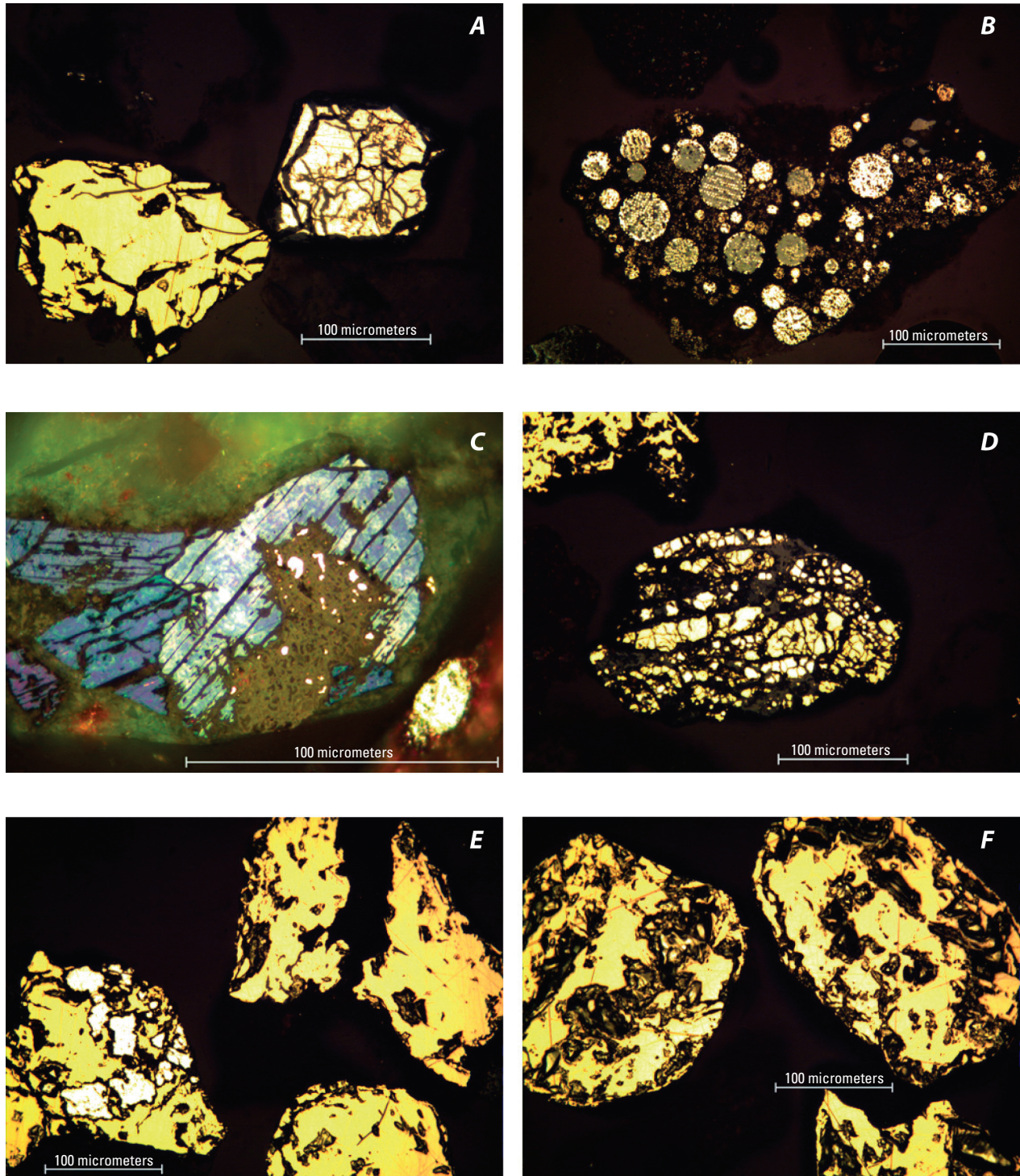


Figure 22. Photographs of variably altered pyrite and chalcopyrite grains in the magnetic fraction of the 60–120 mesh size fraction of tailings sample T1 (A–F), and in downstream sediment S5 (G–K), and S6 (L). Note scale bars for reference. (A) Pitted chalcopyrite (left) and more altered pyrite (?) (right) showing a rim and fracture fillings of iron oxides, (B) pyrite framboids variably altered to iron oxides and suspended in a matrix of quartz and organic matter, (C) rare bornite grains showing characteristic blue color under reflected light, (D) pyrite cemented by iron oxides and quartz, (E) cluster of pitted chalcopyrite grains including one composite grain (left) containing pyrite inclusions, (F) cluster of chalcopyrite grains, (G) angular grain of chalcopyrite, (H) pyrite grain showing extensive replacement by iron oxides, (I) chalcopyrite with a thick rim of banded silica and iron oxide, (J, K) relatively unaltered chalcopyrites, (L) organic-bearing grain with abundant rounded microinclusions of pyrite.

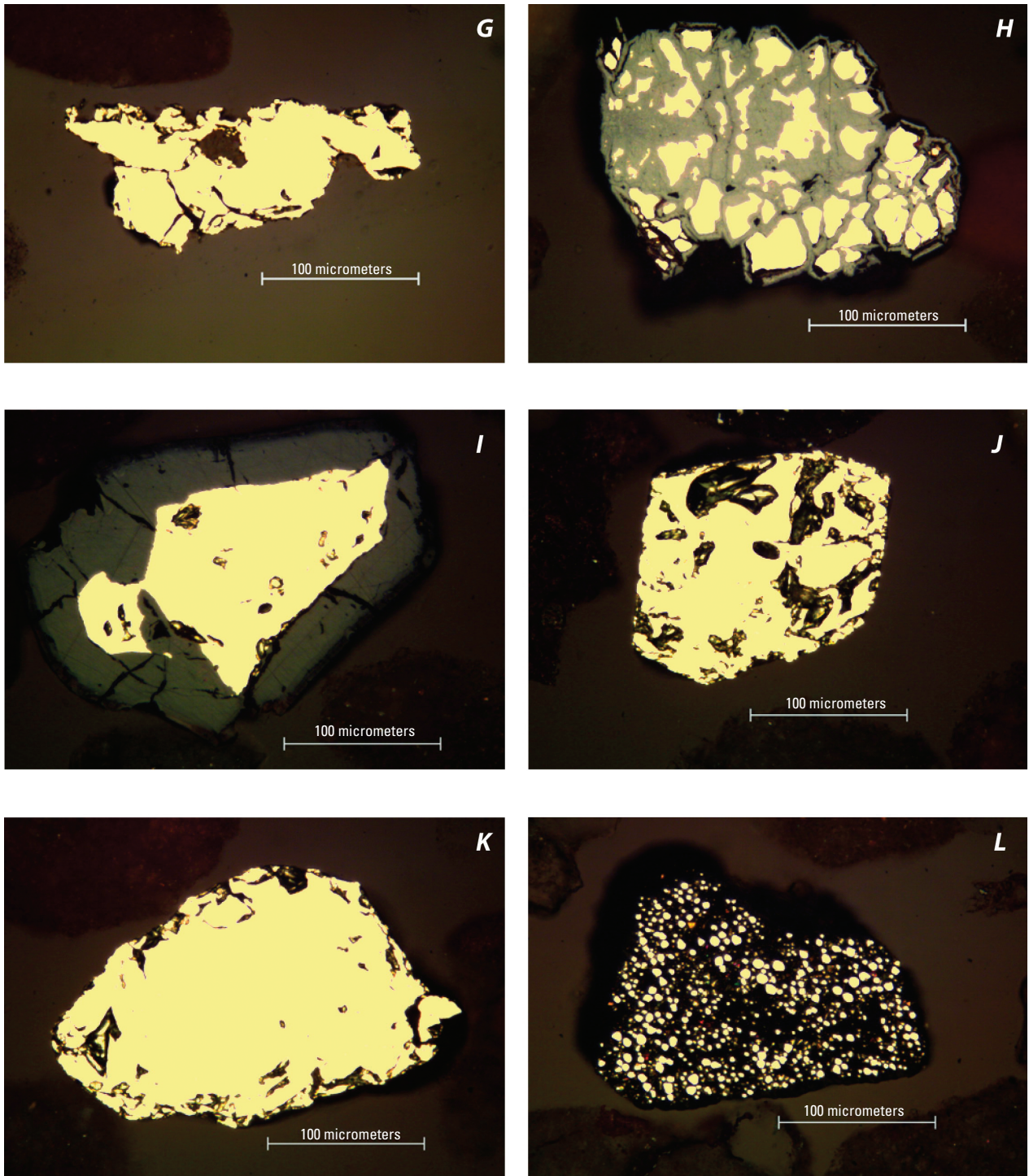


Figure 22—Continued. Photographs of variably altered pyrite and chalcopyrite grains in the magnetic fraction of the 60–120 mesh size fraction of tailings sample T1 (A–F), and in downstream sediment S5 (G–K), and S6 (L). Note scale bars for reference. (A) Pitted chalcopyrite (left) and more altered pyrite (?) (right) showing a rim and fracture fillings of iron oxides, (B) pyrite framboids variably altered to iron oxides and suspended in a matrix of quartz and organic matter, (C) rare bornite grains showing characteristic blue color under reflected light, (D) pyrite cemented by iron oxides and quartz, (E) cluster of pitted chalcopyrite grains including one composite grain (left) containing pyrite inclusions, (F) cluster of chalcopyrite grains, (G) angular grain of chalcopyrite, (H) pyrite grain showing extensive replacement by iron oxides, (I) chalcopyrite with a thick rim of banded silica and iron oxide, (J, K) relatively unaltered chalcopyrites, (L) organic-bearing grain with abundant rounded microinclusions of pyrite.

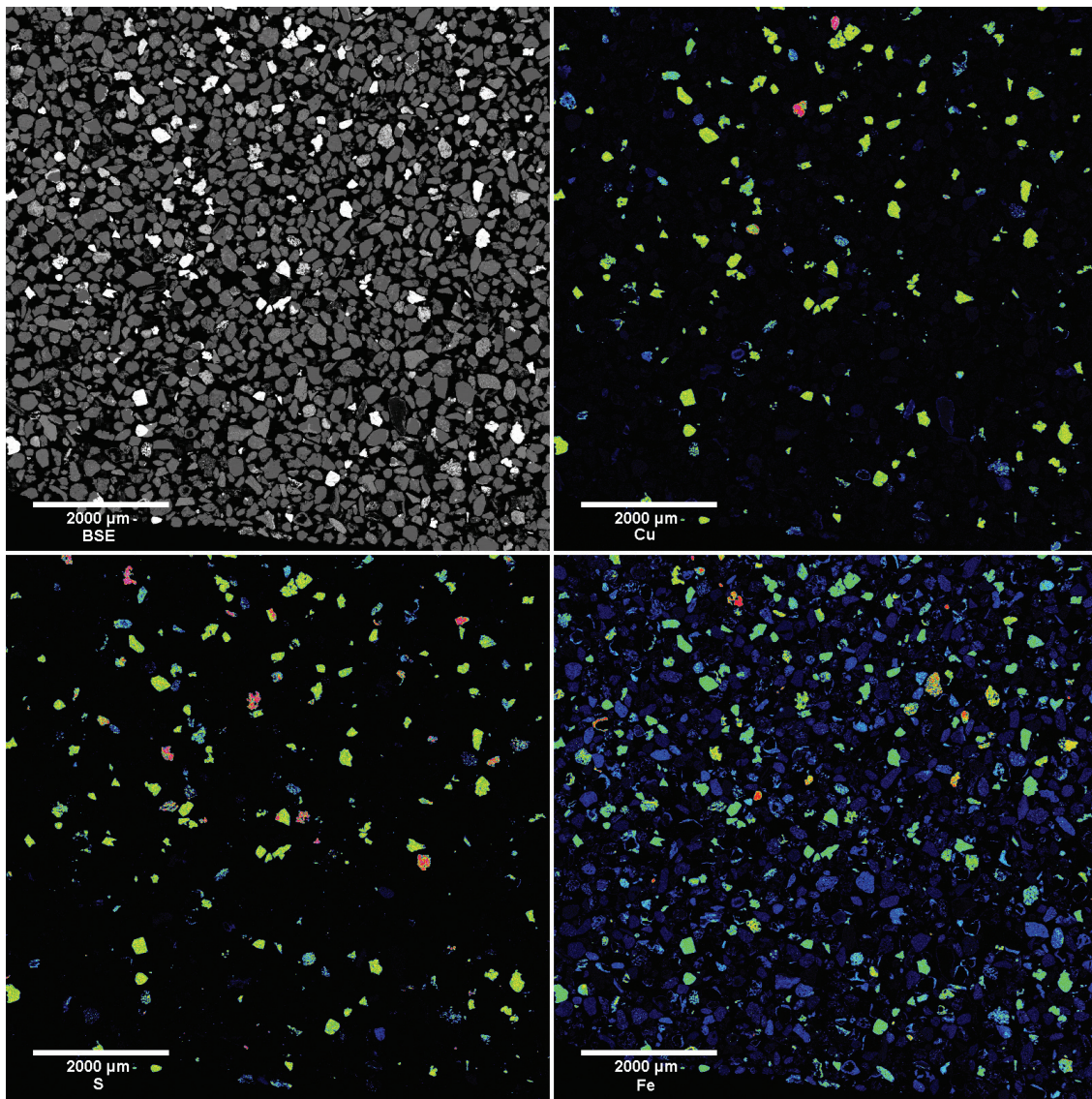


Figure 23. Backscatter electron image (BSE) (upper left) and corresponding X-ray intensity maps for copper, sulfur, and iron for a portion (8 square millimeters) of thin section T1 containing magnetic minerals from the tailings location. The X-ray intensity maps are displayed on a color scale: low-intensity pixels are represented by blue, and highest intensity areas are represented by red to pink.

Summary and Conclusions

Geologic mapping, cross sections, and resistivity profiles at the Bureau of Land Management Fry Canyon project site in San Juan County, southeastern Utah, show the following:

1. Bedrock is composed of thick eolian sandstone beds and interbedded thinner, fine-grained sandstones and siltstones of the Cedar Mesa Sandstone Member of the Permian Cutler Formation.
2. Thick beds of sandstone form stairstep bedrock ledges on the flanks of the valley of Fry Creek; ore-processing companies used these ledges for siting operations. Some ledges are buried beneath unconsolidated valley-floor deposits.
3. Bedrock is mantled by late Quaternary to Holocene reddish-brown deposits of eolian sand and silty sand, which commonly contain thin lenses of colluvium derived locally from exposed, weathered ledges of the Cedar Mesa sandstone.
4. Along the valley bottom through the study area, older alluvial gravels intertongue with eolian sand deposits and colluvium adjacent to the modern channel of Fry Creek; these sediments fill a paleochannel as much as 1–2 m deeper than the modern channel of Fry Creek.
5. The paleochannel seems to be configured as portrayed in figure 24 based on exposed bedrock outcrop along the modern channel, drilling data, and geophysical profiles.

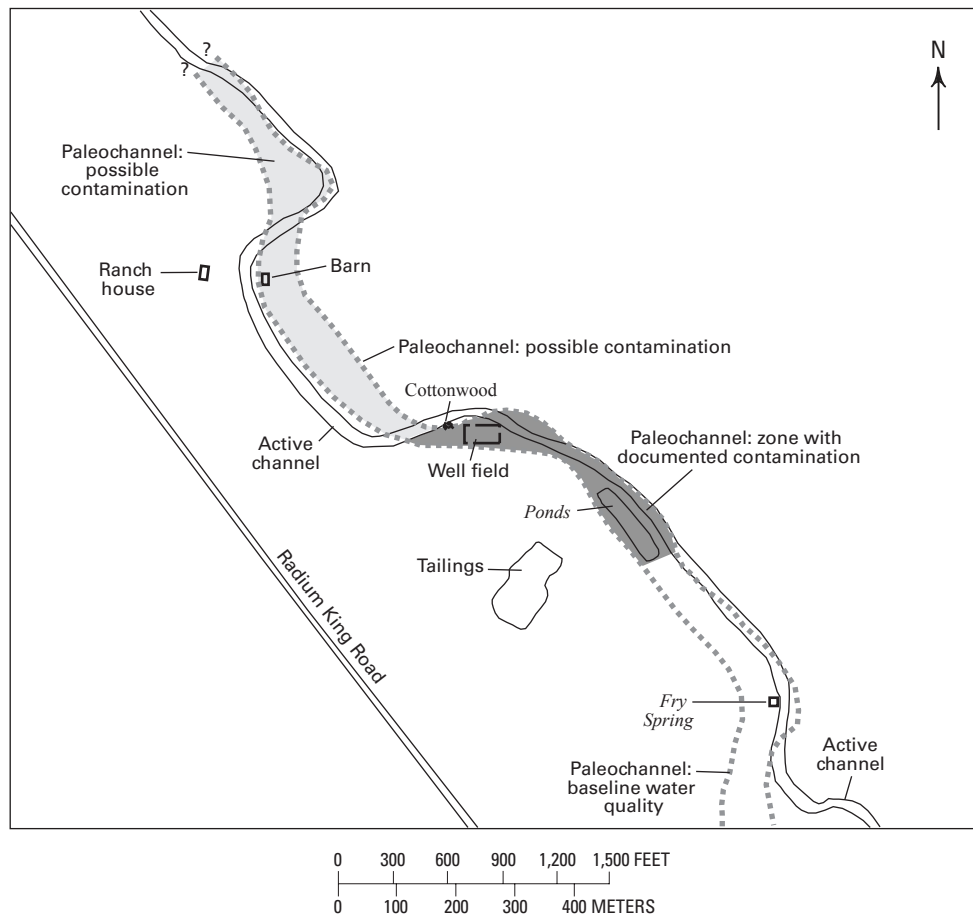


Figure 24. Map of the Fry Canyon project study area showing modern channel and possible position of the paleochannel along the floor of Fry Creek. The light-gray shaded area may include a lower paleochannel and a higher, older paleochannel. This area needs to be tested for sediment thickness and the presence of contaminated groundwater. The older paleochannel north of the barn may contain substantial fresh groundwater.

6. In the vicinity of the ore-processing site, the modern channel of Fry Creek is narrower than this paleochannel; Fry Creek flows on bedrock only locally and alternately follows and crosses the trace of the paleochannel.
7. For at least 0.5 mi (0.8 km) upstream to the south of the Highway 95 bridge, the paleochannel deposits are eroded completely and the modern stream and its thin alluvium rest on bedrock; the northern limit of the paleochannel was not delineated in this study, but it lies north of geophysical profile FC-4.
8. Five of the ponds at the project site sit on a bench composed of eolian sand, colluvium, and gravels of the paleochannel.
9. Groundwater contamination from the ponds and other operations at the site appears to follow the paleochannel and geophysical surveys indicate that the paleochannel extends north to the location of FC-4; however, contamination in paleochannel groundwater may be substantially diluted to the north by influxes of fresher water associated with the modern channel or springwaters along the FC-4 profile.
10. An older, higher paleochannel marked by high-standing gravels is present along part of the stream valley but does not seem to carry contaminated groundwater as it is not in contact with water in the stream or the paleochannels. North of the ranch and barn at the location of FC-4, this channel may contain springwater derived from local bedrock.
11. Groundwater, some of it likely contaminated, has moved into fractured bedrock at selected localities.

Well-water sample W15 collected from the center of the contaminant plume has a distinctive Ca-Mg-SO₄-dominant chemistry that indicates major sourcing of dissolved solids from the heap-leach pile. Other distinctive characteristics of this water include highest dissolved uranium concentration (18,700 µg/L) and markedly more negative δ³⁴S composition (-13.3 per mil), the latter indicating distinctive sources of sulfur provided by the heap-leached Cu-U ores and/or the sulfuric acid leachate.

The ²³⁴U/²³⁸U activity ratios (AR) of uranium in W15 water and nearby well waters influenced by the contaminant plume are all less than 1.0, the result of aggressive, sulfuric acid-based leaching of uranium from Cu-U ore in the heap leach pile. In contrast, the AR values of uranium in waters collected upstream

from the Fry Canyon project site are all greater than 1.0 and result from natural weathering and dissolution of uranium by local waters. This isotopic contrast can be used to identify and quantify the amount of site-derived uranium in well water and surface water collected downstream from the site. Uranium isotopic data provide particularly useful confirmation of uranium contamination in water that has marginally elevated uranium concentrations compared to natural baseline values.

Analysis of copper in the 60- to 120-mesh size fraction of stream sediments provided chemical indications of the downstream dispersion of contaminant chalcopyrite grains. Modern analyses by ICP-MS are highly sensitive and precise, but chemical detection of added chalcopyrite is limited by large dilution factors and natural variability in baseline copper concentrations. In Fry Creek the chemical data confidently indicated addition of chalcopyrite particles at a location 0.1 km downstream from the tailings (S2) but not at 0.4 km downstream (S3).

Optical microscope observations or measurements with the electron microprobe or scanning electron microscope can be used to identify distinctive tailings-derived chalcopyrite grains in thin sections of magnetic mineral concentrates. Chalcopyrite identifications in stream sediments provide a sensitive qualitative indication of downstream dispersion of contaminants, but tracking of rare sulfide grains over large distances is hampered by large dilution factors and nonuniform sampling of stream sediments. In Fry Creek the tailings-derived sulfide particles are greatly diluted by resuspended sediment and sediment newly added during floods. Despite this dilution, tailings-derived sulfide particles were confidently detected at a location (S5) 1.3 km downstream from the streamside tailings.

Use of $^{234}\text{U}/^{238}\text{U}$ activity ratios (AR) to identify uranium contamination in water should be generally applicable at other sites of uranium mining, milling, or processing provided that there is good contrast between the uranium isotopic composition of site-derived uranium and local dissolved uranium. At Fry Canyon and elsewhere, tracing of distinctive site-derived particles such as ore sulfides in stream sediments (or air samplers) is possible by bulk chemical analysis or individual particle identification, but the general success of these methods will depend upon the amount of particle dilution as a function of downstream (or downwind) distance.

Acknowledgments

B.R. Lewis of the Bureau of Land Management encouraged USGS involvement in this study and provided background information, advice, and logistical support. C.A. Rosson and associates at SAIC Engineering, Inc., provided three well-water samples (W18, 19, 20). Uranium isotope data were provided by Professor M.E. Ketterer of Northern Arizona University. Sulfur isotope determinations were by C.A. Johnson; chemical analyses of waters and sediments were by J.H. Bullock, Jr.; and electron microprobe measurements were by H.A. Lowers, all of the USGS. Other USGS employees who contributed technical advice or analytical support are R.L. Driscoll, N.S. Fishman, D.L. Naftz, D.R. Van Sistine, and R.B. Wanty.

References Cited

- Advances Geosciences Inc., 2003, Earth Imager 2D, Resistivity and IP inversion software instruction manual: Advanced Geosciences, Inc., 2121 Geoscience Drive, Austin, Texas, 78726, 92 p.
- Allison, J.D., Brown, D.S., and Novo-Gradac, K.J., 1991, MINTEQA2/PRODEFA2, a geochemical assessment model for environmental systems—Version 3.0 users manual: U.S. Environmental Protection Agency Report EPA/600/3-91/021, 106 p.
- Ball, J.W., and Nordstrom, D.K., 1991, User's manual for WATEQ4F, with revised thermodynamic data base and test cases for calculating speciation of major, trace, and redox elements in natural waters: U.S. Geological Survey Open-File Report 91-183, 189 p.
- Briggs, P.H., 2002, The determination of twenty-seven elements in aqueous samples by inductively coupled plasma-atomic emission spectrometry, *in* Taggart, J.E., ed., Analytical methods for chemical analysis of geologic and other materials, U.S. Geological Survey: U.S. Geological Survey Open-File Report 2002-223, chap. F, p. F1-F11.
- Hem, J.D., 1985, Study and interpretation of the chemical characteristics of natural water: U.S. Geological Survey Water-Supply Paper 2254, 263 p.
- Ho, C.H., and Miller, N.H., 1986, Adsorption of uranyl species from bicarbonate solution onto hematite particles: *Journal of Colloid Interface Science*, v. 110, p. 165-171.
- Hsi, C.K.D., and Langmuir, D., 1985, Adsorption of uranyl onto ferric oxyhydroxides—Application of the surface complexation site-binding model: *Geochimica et Cosmochimica Acta*, v. 49, p. 1931-1941.
- Lamothe, P.J., Meier, A.L., and Wilson, S.A., 2002, The determination of forty-four elements in aqueous samples by inductively coupled plasma-mass spectrometry, *in* Taggart, J.E., ed., Analytical methods for chemical analysis of geologic and other materials, U.S. Geological Survey: U.S. Geological Survey Open-File Report 2002-223, chap. H, p. H1-H11.
- Langmuir, D., 1978, Uranium solution-mineral equilibria at low temperatures with applications to sedimentary ore deposits: *Geochimica et Cosmochimica Acta*, v. 42, p. 547-569.
- Naftz, D.L., Davis, J.A., Fuller, C.C., Morrison, S.J., Felton, E.M., Wilhelm, R.G., Piana, M.J., Joye, J.L., and Rowland, R.C., 1999, Field demonstration of permeable reactive barriers to control radionuclide and trace element contamination in groundwaters from abandoned mine lands, *in* Morganwalp, D.W., and Buxton, H.T., eds., Contamination from hardrock mining, U.S. Geological Survey Toxic Substances Hydrology Program—Proceedings of the Technical Meeting, Charleston, South Carolina, March 8-12, 1999: U.S. Geological Survey Water-Resources Investigations Report 99-4018A, v. 1, p. 281-288.

- Naftz, D.L., Feltcorn, E.M., Fuller, C.C., Wilhelm, R.G., Davis, J.A., Morrison, S.J., Freehey, G.W., Piana, M.J., Rowland, R.C., and Blue, J.E., 2000, Field demonstration of permeable reactive barriers to remove dissolved uranium from groundwater, Fry Canyon, Utah, September 1997 through September 1998, interim report: U.S. Environmental Protection Agency Report EPA 402-C-00-01, 89 p., <http://www.epa.gov/radiation/docs/cleanup/402-c-00-001.pdf>.
- Naftz, D.L., Fuller, C.C., Davis, J.A., Morrison, S.J., Feltcorn, E.M., Rowland, R.C., Freehey, G.W., Wilkowski, C.D., and Piana, M.J., 2002, Field demonstration of three permeable reactive barriers to control uranium contamination in groundwater, Fry Canyon, Utah, USA, in Naftz, D.L., Morrison, S.J., Davis, J.A., and Fuller, C.C., eds., *Handbook of groundwater remediation using permeable reactive barriers—Applications to radionuclides, trace metals, and nutrients*: New York, Academic Press, chap. 14, p. 401–434.
- Naftz, D.L., Fuller, C.C., Snyder, T., and Stolp, B.J., 2006, Permeable reactive barriers—Application to abandoned mine land reclamation in Utah: 2006 National Association of Abandoned Mine Land Programs, 28th Annual Conference, September 25–27, 2006, Billings, Montana, 14 p.
- Osmond, J.K., and Cowart, J.B., 1976, The theory and uses of natural uranium isotope variations in hydrology: *Atomic Energy Review*, v. 14, p. 620–679.
- Parkhurst, D.L., 1995, User's guide to PHREEQC—A computer program for speciation, reaction-path, advective transport, and inverse geochemical calculations: U.S. Geological Survey Water-Resources Investigations Report 95–4227, 143 p.
- Rosenblum, S., and Brownfield, I.K., 1999, Magnetic susceptibilities of minerals: U.S. Geological Survey Open-File Report 99–529, 37 p.
- Thaden, R.E., Trites, A.F., Jr., and Finnell, T.L., 1964, Geology, and ore deposits of the White Canyon area, San Juan and Garfield Counties, Utah: U.S. Geological Survey Bulletin 1125, 166 p.
- U.S. Environmental Protection Agency, 2001, National primary drinking water regulations; radionuclides; final rule: *Federal Register*, v. 65, no. 236, p. 76708–76753.
- U.S. Environmental Protection Agency, 2006a, Current national recommended water quality criteria: Office of Science and Technology Publication EPA-822-H-04-001, <http://epa.gov/waterscience/criteria/wqcriteria.html>.
- U.S. Environmental Protection Agency, 2006b, National drinking water standards: <http://www.epa.gov/safewater/mcl.html#inorganic>.
- Wilkowski, C.D., Rowland, R.C., and Naftz, D.L., 2002, Selected hydrologic data for the field demonstration of three permeable reactive barriers near Fry Canyon, Utah, 1996–2000: U.S. Geological Survey Open-File Report 2001–361, 102 p.

Appendixes

Appendix 1. Description of Disturbed Areas

Disturbed Area at the Ore-Processing Site

Activities at the Fry Canyon site produced an irregular disturbed area (shaded and labeled “d”, fig. 5) about 900 by 900 ft (275 by 275 m). The disturbed area includes the following (locations with number and letter designations shown in fig. 5):

- Six tailings ponds (nos. 1–6), tailings, and contaminated fill that rest on a bench (Qeb) adjacent to Fry Creek;
- One large heap-leach pile (hlp), which apparently rests on thin Qec;
- Substantial areas of slope wash from the eroding banks of the heap-leach pile (marked by arrows);
- Several piles of copper ore that rest on thin Qec or sandstone (“ore” and “ore piles”);
- Several concrete leach vats and other metal recovery features (f) that rest on sandstone ledges;
- Large bulldozed areas where native soils are disturbed (d) and sandstone bedrock (ss) is commonly exposed;
- Ponded stream sediment (ps, upslope side of access road);
- Radioactive slime pile (s);
- Linear pile of bulldozed sandstone rubble (r);
- Pile of rusted scrap iron (m);
- Erosional gullies (two arrowed lines); and
- Other small ponds (nos. 7, 8, 9).

Most of the listed features show varying amounts of radioactivity, each above the background levels observed at the site (1.5–2.5 $\mu\text{R/hr}$ (microroentgen per hour) for units Pcc and Pcb, and 2.5–4.0 $\mu\text{R/hr}$ for unit Qec).

Other Disturbed Areas

West of the access road to the site and just west of the ore-processing area is a large pile of debris that includes remnants of trailers, old equipment, and other waste (j, fig 5). To the northeast of Fry Creek, opposite the main area of

disturbance, is a “cowboy” shack (cs, fig. 5) and an old foundation (f, fig. 5). Remnants of roads and the foundation of a smaller structure (not mapped) are in this area. No anomalous radioactivity was noted at these sites. The northwest-trending linear map area of unit Pcb, surrounded by unit Qeb to the northeast and across the creek from pond 5, has several piles of radioactive ore and slimes sitting on the sandstone bald.

A substantial disturbed area, located around the ranch north of the project site, is associated with the access roads to the ranch house, a car shed, a barn, and a bulldozed area (rh, cs, b, and d, fig. 4). The area around the barn is fenced (dash-dot line, fig. 4), and the bench (Qeb) surface that extends southeast of this fenced area almost to a large cottonwood tree is also fenced (not shown).

Two berms along the stream bottom form small ponds for stock use (w, fig. 4) adjacent to the barn. Five areas with piles of uranium ore or remnants of such piles are located adjacent to road surfaces just to the southwest of the ranch house (ore, fig. 4). Some of this material washes across the main entry road surface (mer, fig. 4). The piles range from a few hundred to more than 5,000 $\mu\text{R/hr}$ (limit of the instrument), thereby posing some hazard to local residents and visitors.

In the Fry Spring area south of the project site (fig. 6), a road provides access to the spring (FS, fig. 6), which is on a stream terrace on the west side of Fry Creek. The spring was developed by digging a rectangular pit with a backhoe into the stream terrace alluvium to depths below the water table. The stream terrace contains a substantial zone of groundwater seeps, and there is a small natural spring in the bottom of a small wash at the southern end of this stream terrace. Groundwater at this locality is believed to be derived from the area of mapped upland Qec that lies west and south of the stream terrace. A large disturbed area (d, fig. 6) lies on the east side of the creek on a bench formed by a ledge of sandstone. A pit and trench (t) are located west of Fry Spring (fig. 6), and other features, such as a dugout and building foundations (not shown), are located on Qeb and sandstone ledges west and northwest of Fry Spring. An old road extends back to the ore-processing site from the Fry Spring access road near the spring to the northwest.

Appendix 2. Apparent-Resistivity Pseudosections and Inversion Results for The Fry Canyon Resistivity Lines

Figures 25–28 in this Appendix provide further information regarding the four geophysical profiles in figures 10, 11, 12, and 13, respectively. The data plots are in EarthImager 2D format (Advances Geosciences Inc., 2003). Each plot has three panels. The top panel shows the measured apparent-resistivity pseudosection and data points. The middle panel shows the calculated apparent-resistivity pseudosection, based on the

inversion results. The bottom panel shows the topography-corrected, inverted resistivity section. Note the color scale varies from plot to plot, and the horizontal and vertical scales are significantly different. Gaps in the subsurface data are shown by missing points in the first two panels. Cross-section areas with substantial data gaps result in poorly constrained model resistivity values in the final figures.

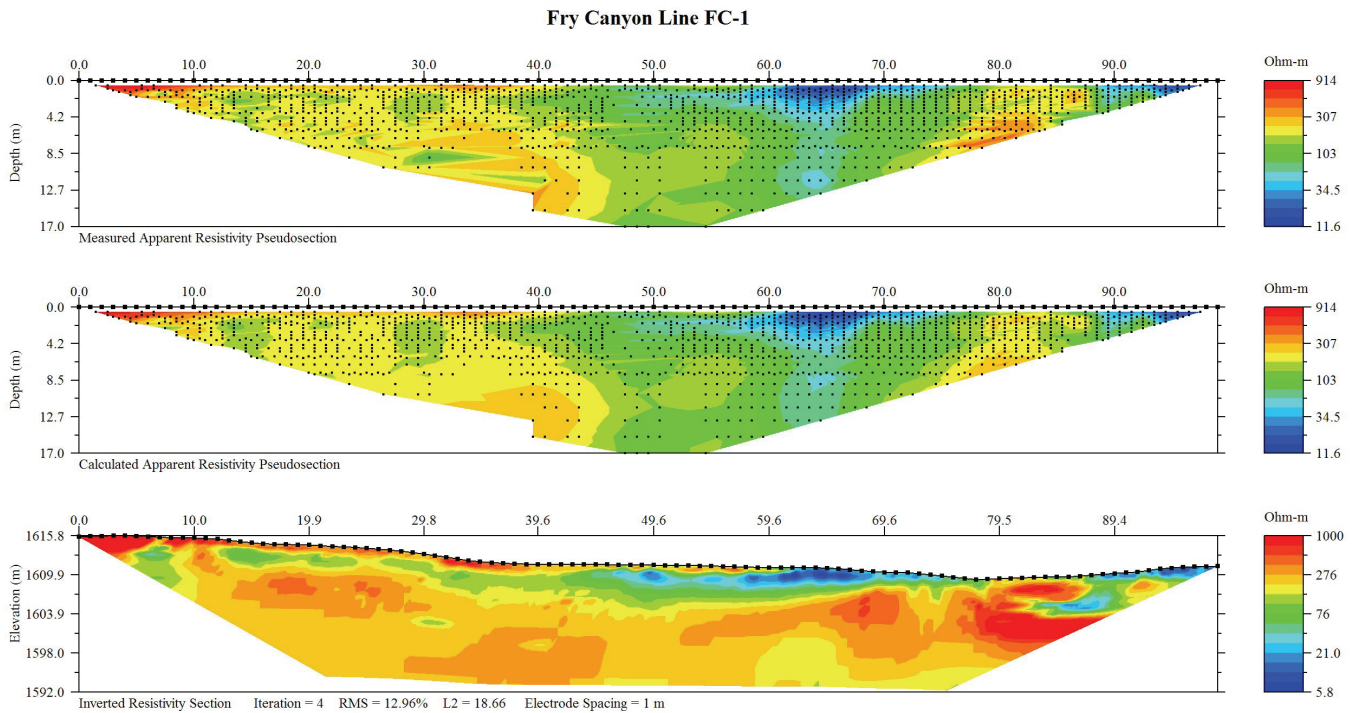


Figure 25. Supporting information for direct-current resistivity profile FC-1. See figure 10 and explanation of the panels in the section on direct-current resistivity surveys.

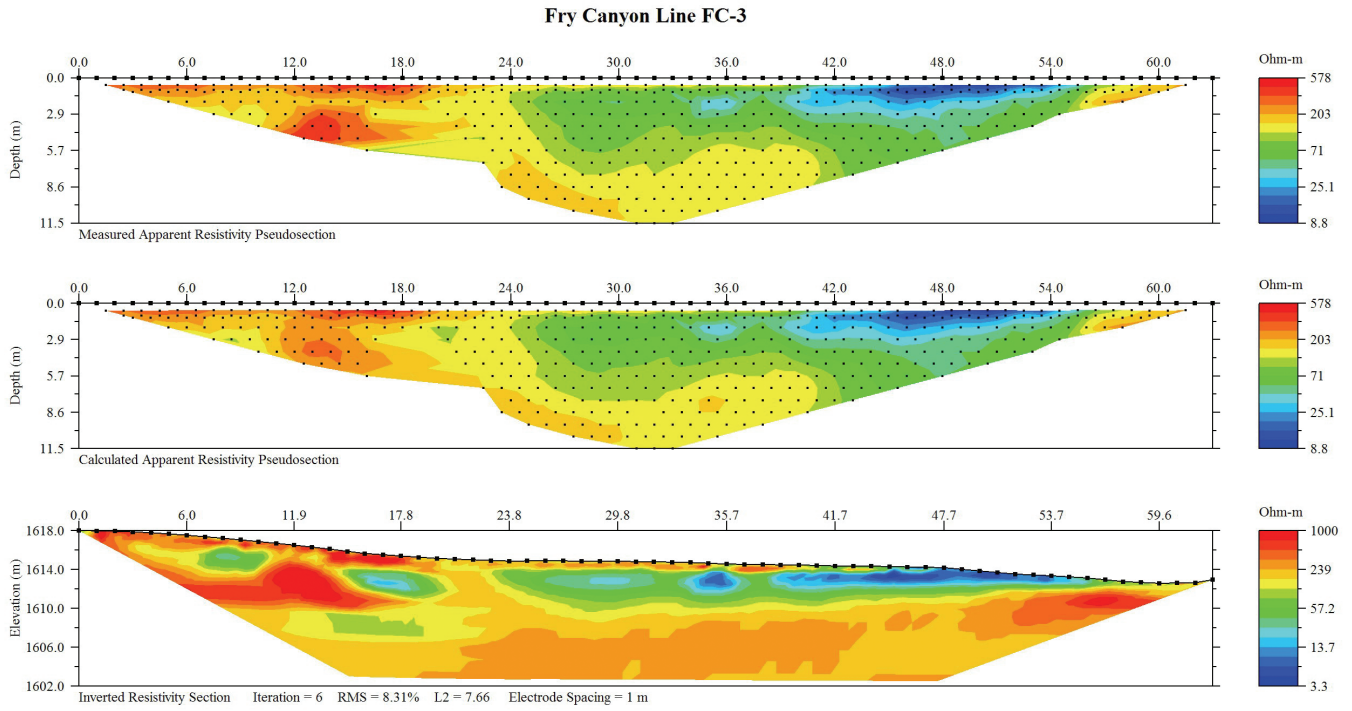


Figure 26. Supporting information for direct-current resistivity profile FC-3. See figure 11 and explanation of the panels in the section on direct-current resistivity surveys.

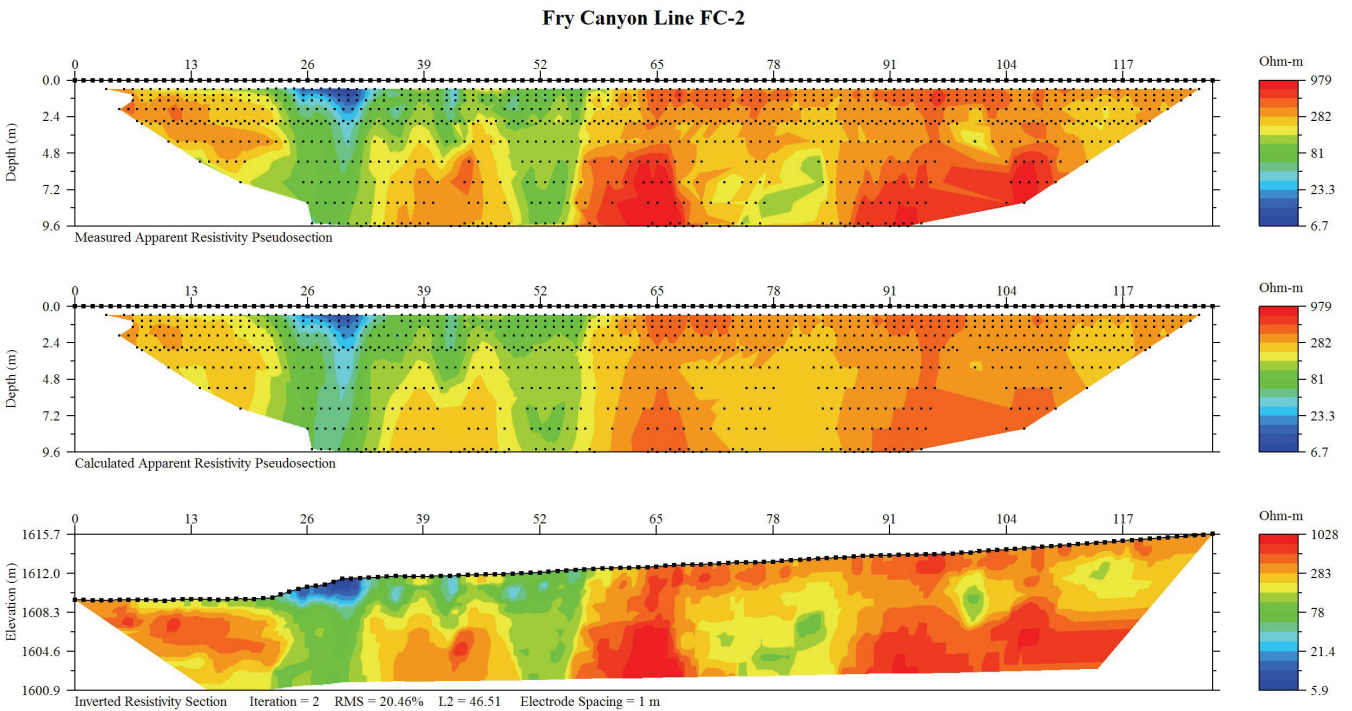


Figure 27. Supporting information for direct-current resistivity profile FC-2. See figure 12 and explanation of the panels in the section on direct-current resistivity surveys.

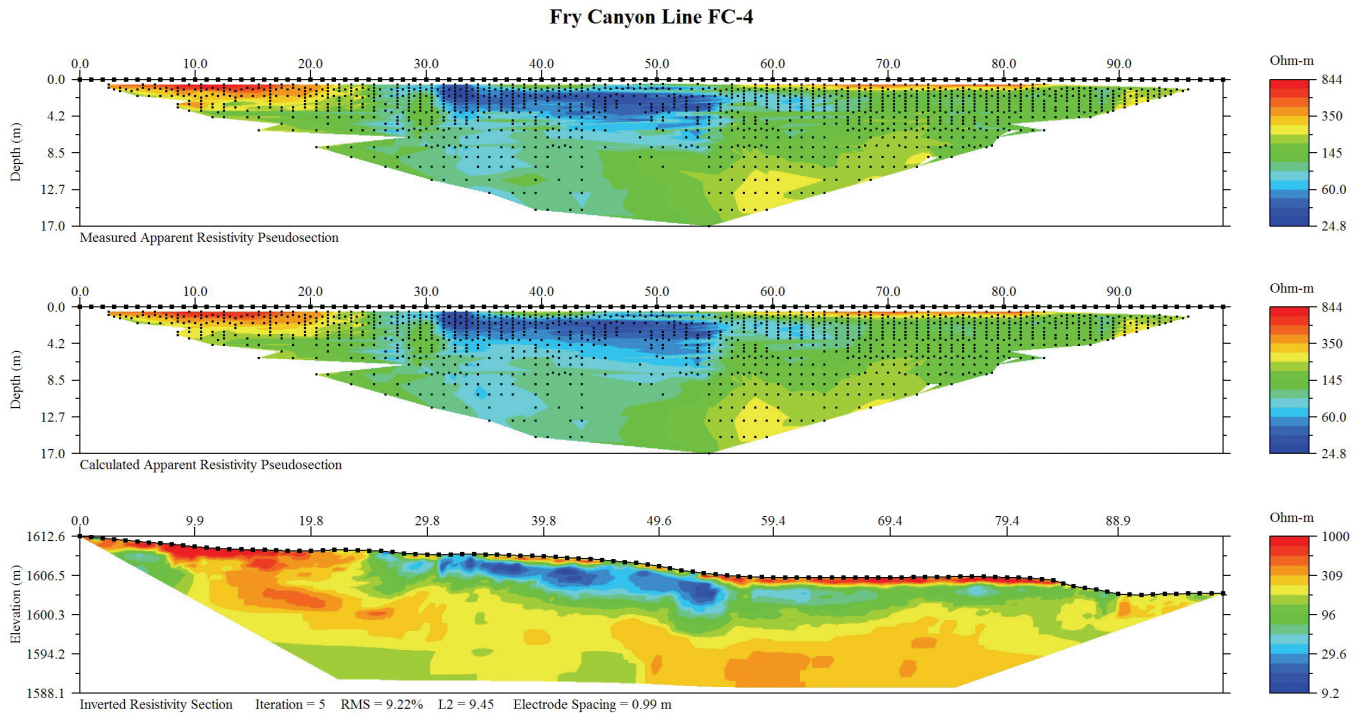


Figure 28. Supporting information for direct-current resistivity profile FC-4. See figure 13 and explanation of the panels in the section on direct-current resistivity surveys.

Publishing support provided by:
 Denver Publishing Service Center, Denver, Colorado
 Manuscript approved for publication, April 3, 2010

For more information concerning this publication, contact:
 Center Director, USGS Central Energy Resources Science Center
 Box 25046, Mail Stop 939
 Denver, CO 80225
 (303) 236-1647

Or visit the Central Energy Resources Science Center Web site at:
<http://energy.cr.usgs.gov/>

This publication is available online at:
<http://pubs.usgs.gov/sir/2010/5075/>

ISBN 978-1-4113-2946-1



9 781411 329461

